NIH Public Access
Author Manuscript
J Magn Reson. Author manuscript; available in PMC 2015 April 01.

Published in final edited form as:
J Magn Reson. 2014 April ; 241: 3–17. doi:10.1016/j.jmr.2014.01.008.

Chemical exchange in biomacromolecules: Past, present, and future

Arthur G. Palmer III*
Department of Biochemistry and Molecular Biophysics, Columbia University, 630 West 168th Street, New York, NY 10032, United States

Abstract

The perspective reviews quantitative investigations of chemical exchange phenomena in proteins and other biological macromolecules using NMR spectroscopy, particularly relaxation dispersion methods. The emphasis is on techniques and applications that quantify the populations, interconversion kinetics, and structural features of sparsely populated conformational states in equilibrium with a highly populated ground state. Applications to folding, mol ecular recognition, catalysis, and allostery by proteins and nucleic acids are highlighted.

Keywords

Proteins; Nucleic acids; Relaxation; NMR; Dynamics; Kinetics

1. Introduction

Time-dependent modulations of nuclear spin resonance frequencies give rise to chemical exchange phenomena in NMR spectroscopy [1]. Chemical exchange affects resonance positions, intensities, and linewidths in NMR spectra; conversely, the importance of chemical exchange for interrogating kinetic or other time-dependent processes has been recognized for decades [2,3]. Use of chemical exchange phenomena as probes of dynamic processes in biological macromolecules, such as proteins and nucleic acids, was for many years hindered by the complexity of ^{1}H spectra [4] and the insensitivity of natural abundance ^{13}C or ^{15}N spectra [5]. The former obstacle has been alleviated by methods for selective protonation of specific sites in otherwise deuterated molecules and the latter by methods for uniform or selective isotopic enrichment with ^{13}C or ^{15}N isotopes (in many applications both approaches are employed, *vide infra*). Isotopic enrichment with ^{13}C or ^{15}N became feasible first and chemical exchange line broadening was quantified in initial studies by multidimensional NMR spectroscopy of protein dynamics as an excess contribution to the ^{15}N transverse relaxation rate constant [6]:

© 2014 Elsevier Inc. All rights reserved.

*Fax: +1 212 305 7932. agp6@columbia.edu.

Note added in proof

The relationship between CEST and low-field $R_{1\rho}$ experiments also has been highlighted in B. Zhao, A.L. Hansen, Q. Zhang, Characterizing slow chemical exchange in nucleic acids by carbon CEST and low spin-lock field $R_{1\rho}$ NMR spectroscopy, J. Am. Chem. Soc., **136** (2014) 20–23.

NIH-PA Author Manuscript
NIH-PA Author Manuscript
NIH-PA Author Manuscript

NIH-PA Author Manuscript

NIH-PA Author Manuscript

NIH-PA Author Manuscript

$$R_2 = R_2^0 + R_{ex} \quad (1)$$

in which R_2 is the observed free-precession transverse relaxation rate constant, R_2^0 is the relaxation rate constant in the absence of chemical exchange (dominated by dipole–dipole, chemical shift anisotropy, and quadrupolar relaxation mechanisms in biological macromolecules [1]), and R_{ex} is the chemical exchange relaxation contribution. Eq. (1) assumes that R_{ex} is independent of R_2^0, a situation that applies if the kinetic rate constants for chemical exchange are large compared to the difference in values of R_2^0 for the exchanging chemical species (*vide infra*). In addition, the value of R_{ex}, and hence R_2, may depend on radiofrequency (rf) fields applied during the NMR experiment, most commonly as spin-echo trains, spin-lock pulses, or adiabatic sweeps [7]. Qualitative identification of sites of exchange broadening using Eq. (1) remains an important part of many investigations, allowing rationalization of weak or missing resonance signals that hinder assignments and structure determination and identifying contiguous regions of higher flexibility that may be linked to function [8-11].

Experimental methods directly aimed at quantifying chemical exchange, generally by making use of the rf field dependence of R_{ex}, enable detailed characterization of structures, kinetics, and equilibria of interconverting species, even with populations less than a few percent in solution. These studies originated with applications to ^{13}C and ^{15}N labeled proteins [12-14]; more recently, methods have been developed that allow characterization of exchange broadening of ^{1}H resonances, making use of the large magnetogyric ratio of the ^{1}H spin, while minimizing the complex effects of ^{1}H spin interactions [15-18].

This *Perspective* briefly reviews these past and present achievements and suggests areas of future interest in quantitative investigation of chemical exchange phenomena in proteins and other biological macromolecules. The *Perspective* highlights experimental methods for solution NMR spectroscopy that have been developed recently and illustrates applications of these methods with some examples drawn from my own laboratory. A major theme of the *Perspective* is the development and application of spin-locking methods for probing a wide range of kinetic time scales. Methods for investigations of biomacromolecular conformational dynamics in solid-state NMR are rapidly developing and have many parallels with solution NMR methods (for a recent review, see [19]).

2. Theory

Chemical exchange in NMR spectroscopy is treated theoretically using the Bloch–McConnell equations for Bloch magnetization components (M_x, M_y, M_z) or more generally the Stochastic Liouville Equation (SLE) for arbitrary elements of the density operator [20]. These equations can be formally written as:

$$\frac{d}{dt}\boldsymbol{\rho}(t) = (-i\boldsymbol{L} - \hat{\boldsymbol{\Gamma}} + \Xi)\,\boldsymbol{\rho}(t) \quad (2)$$

in which $\boldsymbol{\rho}(t) = [\boldsymbol{\rho}_1(t), \boldsymbol{\rho}_2(t), \ldots, \boldsymbol{\rho}_N(t)]^T$ is the density matrix in the Liouville representation with dimension $(M \cdot N) \times 1$ (understood as the difference from the equilibrium density

NIH-PA Author Manuscript

NIH-PA Author Manuscript

NIH-PA Author Manuscript

operator); M is the dimension of the spin space; N is the number of exchanging chemical states; $\boldsymbol{\rho}_k(t)$ is the density operator for the kth chemical state; $\boldsymbol{L}$ and $\hat{\boldsymbol{\Gamma}}$ are the Liouvillian and relaxation superoperators, respectively, defined as:

$$\boldsymbol{L}=\begin{bmatrix} \boldsymbol{L}_1 & 0 & \cdots & 0 \\ 0 & \boldsymbol{L}_2 & \cdots & 0 \\ \vdots & \vdots & \ddots & \vdots \\ 0 & 0 & \cdots & \boldsymbol{L}_N \end{bmatrix} \quad (3)$$

$$\hat{\boldsymbol{\Gamma}}=\begin{bmatrix} \hat{\boldsymbol{\Gamma}}_1 & 0 & \cdots & 0 \\ 0 & \hat{\boldsymbol{\Gamma}}_2 & \cdots & 0 \\ \vdots & \vdots & \ddots & \vdots \\ 0 & 0 & \cdots & \hat{\boldsymbol{\Gamma}}_N \end{bmatrix} \quad (4)$$

$\boldsymbol{L}_k$ and $\hat{\boldsymbol{\Gamma}}_k$ are the $M \times M$ Liouvillian and relaxation superoperators in the spin space for the kth chemical state; $\boldsymbol{\Xi} = \mathbf{K} \otimes \mathbf{E}$; $\mathbf{K}$ is the $N \times N$ matrix of kinetic rate constants; $\mathbf{E}$ is the $M \times M$ identity matrix; $K_{ij} = k_{ji}$ ($i \neq j$); $K_{ii} = -\sum_{j=1}^{N} k_{ij}$; and k_{ij} is the (pseudo-first-order) rate constant for transition from chemical state i to j. The dimensionality of the Bloch–McConnell and Stochastic Liouville Equations grows rapidly with either the size of the spin system or number of exchanging states; consequently, exact closed-form solutions are available for few situations. Modern computers permit numerical solutions of the SLE for arbitrary cases and software programs are available for data analysis [21,22]. Nonetheless, approximate analytical solutions for limiting cases, such as fast kinetic exchange or highly skewed state populations, continue to be useful for both qualitative understanding and data analysis. For example, when $N = 2$ and the site populations satisfy $p_1 \gg p_2$, i.e. one chemical state is dominant, the perturbation approach of Trott and Palmer gives the free-precession relaxation rate constant as $R_2 = R_{21}^0 + R_{ex}$ in which:

$$R_{ex} = \frac{k_{12}\left\{\Delta\omega^2 + \Delta R_2^0\left(k_{21} + \Delta R_2^0\right)\right\}}{\left(k_{21} + \Delta R_2^0\right)^2 + \Delta\omega^2} \quad (5)$$

and $\Delta R_2^0 = R_2^0 - R_{21}^0$ [23]. In this case, in contrast to Eq. (1), the exchange broadening is not independent of the exchange-free relaxation rate constants R_{2i}^0 (and this result can be generalized to N-state exchange).

3. ZZ-exchange spectroscopy

The first heteronuclear experiments specifically intended for characterizing chemical exchange in biological macromolecules were based on concepts from ^{1}H EXSY and ^{1}H–X (X = ^{13}C or ^{15}N) HMQC or HSQC heteronuclear correlation experiments. Like ^{1}H EXSY [24], these so-called ZZ-exchange experiments are appropriate for slow chemical exchange in which resolved resonances are observed for the individual chemical states. Initial experiments by Montelione and Wagner used $2I_zS_z$ longitudinal two-spin order or S_z magnetization (I = ^{1}H, S = ^{13}C or ^{15}N) during the mixing period, rather than I_z

NIH-PA Author Manuscript

NIH-PA Author Manuscript

NIH-PA Author Manuscript

magnetization as in ^{1}H EXSY [25]. Subsequent developments by Wüthrich and coworkers [26] and Kay and coworkers [27] led to a widely used pulse sequence for heteronuclear ZZ-exchange spectroscopy using S_z magnetization during the mixing time and HSQC-style frequency labeling. This pulse sequence is shown in Fig. 1a. An example of ZZ-exchange data for the two-state monomer–dimer equilibrium for a protein construct comprising extracellular domains 1 and 2 of mouse E-cadherin is shown in Fig. 2 [28]. These data were analyzed using a composite peak intensity ratio defined by [29]:

$$\Pi(T) = \frac{I_{ij}(T)\, I_{ji}(T)}{I_{ii}(T)\, I_{jj}(T) - I_{ij}(T)\, I_{ji}(T)} = k_{12}\, k_{21}\, T^2 \quad (6)$$

in which $I_{ij}(T)$ is the intensity of the crosspeak ($i \neq j$) or diagonal peak ($i = j$) in the spectrum recorded with a mixing time T. This expression both simplifies data analysis and is less sensitive to differences in relaxation rates for (monomer and dimer) exchanging species. To independently determine k_{12} and k_{21}, the equilibrium constant K_D is determined from fully relaxed correlation spectra; for accurate results, the effects of differential relaxation during coherence transfer periods must be considered [7,30].

For proteins that are ^{15}N labeled and deuterated at non-exchangeable sites, ^{15}N TROSY-selected [31] and TROSY-detected [32] ZZ-exchange experiment have been described. In this and other TROSY-based experiments [33], TROSY-selected methods measure the relaxation rate constant of the TROSY resonance (e.g. $I^{\beta}S_z$ or $I^{\beta}S^{+/-}$) and detect using a two-dimensional TROSY sequence. In contrast, TROSY-detected methods measure the relaxation rate constant of in-phase magnetization and detect using a TROSY sequence. TROSY-selected experiments have the advantage of reduced intrinsic relaxation rate constants (*vide infra*), although fast amide proton solvent exchange compromises sensitivity. The pulse sequence for the TROSY-selected experiment is shown in Fig. 1b. This pulse sequence has been employed by Henzler-Widman and coworkers as part of an investigation of the small multi-drug resistance transporter EmrE in bicelles, showing that the protein exchanges between asymmetric dimeric conformations associated with inward and outward facing states of the transporter in membranes [34].

Although ZZ-exchange spectroscopy is now a well-established technique, the method is limited in two ways: (i) the chemical shifts of resonances must be resolved in the various chemical states and (ii) exchange kinetics must be faster than the relaxation rates of the magnetizations or coherences present during the mixing time of the pulse sequence. In some instances, resonances for certain nuclear spin types may be better resolved than others. For example, the X-nucleus frequency labeling periods shown in Fig. 1 can be replaced with ^{1}H spin evolution periods or the experiments extended into a third frequency dimension [35]. Alternatively, if the macromolecule of interest is weakly aligned in liquid crystalline media, a difference in resonance frequencies for a selected multiplet component may be observed, even in the absence of a chemical shift difference, owing to differences in residual dipolar couplings (RDCs) in different chemical states [36,37]. An example is shown in Fig. 3 for the small molecule N,N-dimethyltrichloroacetamide (DMTCA), which undergoes hindered rotation exchanging the two methyl groups. A ZZ-exchange experiment with a ^{1}H inversion pulse during the t_1 frequency-labeling interval shows the conventional pattern of auto- and

NIH-PA Author Manuscript

NIH-PA Author Manuscript

NIH-PA Author Manuscript

cross-peaks (Fig. 3b). If decoupling is omitted during t_1, the multiplet patterns in each state are determined by the sum of the scalar and residual dipolar couplings (Fig. 3a). If ^{13}C chemical shift evolution during t_1 is suppressed intentionally, ZZ-exchange cross peaks are still observable for the upfield and downfield multiplet components reflecting differences in RDCs for the two methyl positions (Fig. 3c). Singlet states, which have relaxation rates many times smaller than conventional *z*-magnetization or longitudinal two-spin order, have been shown to allow detection of very slow chemical exchange processes [38]. Routine applications to proteins or other biological macromolecules await appropriate isotopic labeling and pulse sequence schemes for selective excitation of singlet states in proteins and other biological macromolecules.

4. CPMG and $R_{1\rho}$ relaxation dispersion

The greatest degree of development in the use of chemical exchange phenomena in biological macromolecules has occurred for the technique of relaxation dispersion, in which relaxation rate constants are measured as functions of applied rf fields. These experiments are utilized when exchange kinetics are too fast or populations of the higher-energy states are too low to observe resolved resonances for the individual chemical states. In these situations a single resonance is observed, reflecting the population-averaged chemical shift for fast exchange, or the major highly populated species for slow exchange. Two principle experimental approaches exist: in one, a windowed Carr–Purcell–Meiboom–Gill (CPMG) train of 180° rf pulses is applied during the relaxation delay; in the other, a windowless rf field (which may be amplitude or phase modulated) is utilized [7,39]. In the CPMG approach, the dispersion of transverse relaxation rate constants, R_2, is measured as a function of the inter-pulse delay, τ_{cp}. In the other approach, dispersion of $R_{1\rho}$ relaxation rate constants is measured as a function of the effective field in the rotating frame, by varying the rf amplitude or frequency; related techniques based on $R_{2\rho}$ relaxation also have been described [40,41]. Although many analytical solutions have been derived for the exchange contribution to relaxation in CPMG [42-45] and $R_{1\rho}$ experiments [23,39,46-49], for the present discussion, only approximations for two-site exchange in which the equilibrium site populations of the two chemical states satisfy $p_1 \gg p_2$ are given to illustrate the two experiments [45,46]:

$$R_{ex}=\frac{p_1 p_2 \Delta\omega^2}{k_{ex}}\left[\frac{k_{ex}^2}{k_{ex}^2+\omega_e^2}\right] \quad (7)$$

in which $k_{ex} = k_1 + k_2$, $\Delta\omega = \Omega_2 - \Omega_1$; Ω_k is the resonance offset frequency in the *k*th state;

$$\begin{array}{rcl} \omega_e^2 & = & [144/\tau_{cp}^4+p_2^2\Delta\omega^4]^{1/2} \quad (CPMG) \\ \omega_e^2 & = & \omega_{1,eff}^2\omega_{2,eff}^2/\omega_{eff}^2 \quad (\mathrm{R}_{1\rho}) \end{array} \quad (8)$$

$\omega_{eff}=(\overline{\Omega}^2+\omega_1^2)^{1/2}$ is the effective field in the rotating frame for the population-average resonance offset frequency, $\overline{\Omega}$; $\omega_{k,eff}=\left(\Omega_k^2+\omega_1^2\right)^{1/2}$ is the corresponding effective field for the *k*th chemical state; and ω_1 is the amplitude of the spin-lock rf field. The dependence of R_{ex} on kinetic parameters is illustrated in Fig. 4. The total transverse relaxation rate constant

NIH-PA Author Manuscript

NIH-PA Author Manuscript

NIH-PA Author Manuscript

for the CPMG experiment is obtained by substituting Eq. (7) into Eq. (1). The observed relaxation rate constant in the tilted reference frame of the $R_{1\rho}$ experiment is obtained as:

$$R_{1\rho}=R_1\, cos^2\theta+(R_2^0+R_{ex})\, sin^2\,\theta \quad (9)$$

in which tan $\theta = \omega_1/\bar{\Omega}$ The expressions in Eqs. (1) and (7)-(9) assume that transverse relaxation rate constants R_{2k}^0 are identical in both chemical states. The effects of violations of this assumption have been discussed and are small if $|\Delta R_2^0| \ll k_{ex}$ [49,50]. The limit in which R_2^0 for the sparsely populated state is extremely large forms the basis for the Dark-state Exchange Saturation Transfer (DEST) experiment (*vide infra*) [51]. In the fast exchange limit ($k_{ex} > \Delta\omega$), CPMG and $R_{1\rho}$ experiments yield very similar dispersion profiles and allow extraction of two parameters, $p_1p_2\Delta\omega^2$ and k_{ex} by fitting to the experimental data. When exchange is intermediate-to-slow ($k_{ex} < \Delta\omega$), both experiments allow determination of p_1p_2 separately from $\Delta\omega$. In addition, the $R_{1\rho}$ relaxation rate constant depends on the resonance offset of spins in the sparsely populated state, because $\omega_e^2 \rightarrow \Omega_2^2+\omega_1^2$; thus, the $R_{1\rho}$ approach permits direct determination of the frequencies of the otherwise unobservable resonances. The CPMG experiment depends only on $|\Delta\omega|$; however, when exchange is not in the fast limit, peak shifts in HMQC/HSQC spectra provide information on the absolute sign of chemical shift differences to augment CPMG results [52]. The relative merits of these different approaches for determination of the sign of $\Delta\omega$ have been discussed [53,54].

Some initial pessimism about the viability of CPMG methods for studies of biological macromolecules [55] was eliminated by the development of the relaxation-compensated CPMG pulse sequence [12]. The key insight of this experiment was that the effects of scalar *J*-coupling evolution during the variable inter-pulse spacing in the CPMG pulse train could be averaged by interchanging in-phase and anti-phase spin operators in an IS spin system at the midpoint of the relaxation period. This approach has been applied to other spin systems subsequently, proving its generality [56,57]. An alternative approach has been developed recently, in which ^{1}H continuous-wave decoupling during the CPMG sequence is used to prevent evolution of the scalar coupling altogether [58]. This latter approach is particularly important for systems subject to rapid solvent exchange and has been applied to lysine NH3 groups in proteins [59]. Recoupling artifacts arising from matching between ^{1}H decoupling pulses and X-nucleus spin-lock pulses in $R_{1\rho}$ experiments initially restricted spin-lock field strengths to values much larger than one-bond scalar coupling constants, but redesign of pulse sequences has ameliorated these limitations [60,61]. Modern cryogenically cooled NMR probes also increase the maximum strength of spin-lock fields that can be employed, enabling investigations of faster kinetic processes [62]. Experiments for multiple-quantum, rather than single quantum, coherences also have been described [63-72]. Multiple-quantum relaxation rate constants may be more easily measured than single quantum relaxation rate constants in some instances [70,71] and in general provide information on whether the resonance frequency fluctuations for the spins involved in the multiple quantum coherence are (anti-) correlated [63,73].

Other developments have increased the robustness of relaxation dispersion experiments. Millet and coworkers showed that the static magnetic field dependence of chemical

NIH-PA Author Manuscript

NIH-PA Author Manuscript

NIH-PA Author Manuscript

exchange is important in defining the chemical exchange time scale [74]; global fitting of relaxation dispersion curves recorded at two or more static magnetic fields has proven to be very effective. The values of the relaxation rate constant in the limits of very small (when the full exchange broadening is obtained) and very large (when the exchange broadening is eliminated) effective fields also are important constraints on data analysis. Hahn-echo experiments, in which only one or two spin-echo sequences are utilized, approximate the free-precession limit rate constant [75,76] and a very robust ^{15}N TROSY-selected Hahn-echo sequence has been developed [77]. The large field limit, when all exchange broadening is suppressed, has been approximated by a number of methods, including field-dependence of relaxation rate constants [78], relaxation interference rate constants [79], linear combinations of single- and multiple-quantum relaxation rate constants in spin-locking experiments [69], and joint analysis of CPMG and $R_{1\rho}$ data [80]. An elegant pulse sequence for the latter has been published recently [81], indicating the continued developments in this area.

As for ZZ-exchange experiments, HSQC-detected, TROSY-detected, and TROSY-selected CPMG and $R_{1\rho}$ pulse sequences have been developed for ^{15}N spins; versions of the TROSY-detected [82] and TROSY-selected [83] $R_{1\rho}$ sequences are shown in in Fig. 5 for illustration. Examples of $R_{1\rho}$ data are shown in Fig. 6 for the protein ubiquitin to illustrate the improvement offered by the TROSY-selected pulse sequence because the exchange-free relaxation rate constant for the TROSY component of the ^{1}H-^{15}N doublet satisfies $R_2^{\beta,0}<R_2^0$ [83]. Relaxation dispersion experiments applied to macromolecules in dilute liquid crystalline media also permit measurement of RDCs [36,37] and residual chemical shift anisotropies [84] for sparsely populated states. Relaxation dispersion at multiple static magnetic fields and multiple temperatures, combined with analyses of new X-ray crystal structures and computationally generated ensembles of structures (*vide infra*) have resulted in detailed understanding of the conformational kinetic processes that lead to line broadening in ubiquitin [13,71,72,85,86].

5. ^{13}C and ^{1}H relaxation dispersion

In proteins, ^{15}N spins are convenient probes for chemical exchange processes because (i) these spins are rare so that coupling interactions between ^{15}N spins are weak, (ii) dipole and chemical shift relaxation rates are relatively small and can be reduced further by deuteration and TROSY methods, (iii) isotopic enrichment is straightforward, and (iv) ^{15}N chemical shifts are affected by many magnetic influences. On the other hand, ^{15}N spins have drawbacks as probes: (i) fast solvent exchange of directly bonded hydrogen atoms reduces the efficiency of relaxation methods and (ii) the low magnetogyric ratio of ^{15}N nuclear limits the amplitude of rf fields that can be applied experimentally. Over the past few years, numerous methods have been developed for relaxation dispersion measurements of ^{1}H and ^{13}C spins. These methods rely on schemes for isotopic enrichment that reduce unwanted scalar and dipolar coupling interactions and on pulse sequence designs that minimize systematic interference from residual interactions. Determination of chemical shifts for as many sites and nuclei as possible is important for calculation of structures of sparsely populated states (*vide infra*). Accordingly, methods have been developed for $^{1}H^{N}$

NIH-PA Author Manuscript

NIH-PA Author Manuscript

NIH-PA Author Manuscript

[87-89], $^{1}H^{\alpha}$ [90-92], ^{13}CO [93-95], $^{13}C^{\alpha}$ [92,94,96], and $^{13}C^{\beta}$ [97] spins. Related methods have been developed for aromatic groups, which are relatively rare in proteins but provide additional probes of the hydrophobic core dynamics [98] and side chain ^{1}H spins [18].

An example of $^{1}H^{N}$ CPMG relaxation dispersion for the monomeric form of mouse E-cadherin extracellular domains 1 and 2 is shown in Fig. 7 [28]. The chemical exchange broadening results from formation of a sparsely populated intermediate, termed the “X-dimer” from X-ray studies, that is structurally distinct from the strand-swapped dimer. Comparisons of the wild-type protein with a mutant that blocks formation of the X-dimer establishes that an X-dimer-like state is an on-pathway intermediate for the strand-swapped dimer described in Fig. 2. Thus, the combination of ZZ-exchange and relaxation dispersion techniques allow full kinetic characterization of dimerization of wild-type E-cadherin in solution.

Particularly important developments have been reported using methods based on the special properties of methyl groups. Rapid rotation of the methyl group reduces ^{1}H–^{13}C dipole–dipole relaxation of the ^{13}C group by a factor of ~1/9. In one set of experiments, the AX_3 methyl spin system is simplified to an approximately AX system by random fractional deuteration and selection by pulse sequence design for $^{13}CHD_2$ isotopomers. Methods then exist for measuring chemical exchange of ^{13}C [99] and ^{1}H spins [15-17]; as an example, Fig. 8a shows a recently reported pulse sequence for ^{1}H $R_{1\rho}$ measurements [17]. A variant of this experiment has been applied to methionine methyl groups in the α_7 ring of the 20S proteasome from *T. acidiphilium* [16]. The results indicate that relaxation dispersion to be measured in very large molecular species prepared with protonated $^{13}CH_3$ groups in a highly deuterated background (including stereospecifically deuterating one methyl group in Val and Leu residues) [100]. Fig. 8b shows a related pulse sequence for measurements of ZQ/DQ relaxation rate constants by a methyl-TROSY Hahn-echo sequence that uses ZQ evolution during t_1 and suppresses anti-TROSY multiplet components [70]. Even for large systems, filtration reduces spectral artifacts from methyl groups in flexible or disordered regions.

Fig. 9 illustrates the application of ^{13}C relaxation dispersion measurements to characterize a sparsely populated state of the villin headpiece domain HP67 [96], which has also been investigated by ^{15}N relaxation dispersion [101]. This application used random fractional labeling with ^{13}C to minimize ^{13}C–^{13}C scalar and dipolar interactions. Two different relaxation dispersion approaches were utilized: for $^{13}C^{\alpha}$ spins, CPMG data were acquired at a single static magnetic field and these data were supplemented by Hahn-echo rate constants recorded at five static magnetic fields. The field dependence of the Hahn-echo data was used both to establish the chemical exchange regime and to determine R_2^0 as a constraint for fitting CPMG dispersion curves. For $^{13}CH_3$ methyl groups, CPMG relaxation dispersion was measured at two static magnetic fields and analyzed globally. HP67 consists of an N-terminal subdomain (residues 10–42) that transiently unfolds at equilibrium under native-like conditions and a highly stable C-terminal subdomain (residues 43–76). Comparisons between p_1p_2 $\Delta\omega 2$ and secondary chemical shifts reveal three groupings of residues in the intermediate: (i) residues that are highly disordered, (ii) residues that maintain partial native-like structure, and (iii) residues that make non-native-like interactions. Residues in the

NIH-PA Author Manuscript

NIH-PA Author Manuscript

NIH-PA Author Manuscript

second category are spatially located in the interface between the N- and C-terminal domains and residues in the third category are located in the vicinity of His 41, which can become protonated in the intermediate state.

6. CEST and DEST

Two very similar techniques have been developed to obtain information on chemically exchanging systems in which the exchange time scale is slow and the populations of the sparsely populated states are too low for reliable quantification by CPMG relaxation dispersion or ZZ-exchange methods alone: Chemical Exchange Saturation Transfer (CEST) [102-104] and DEST (*vide supra*) [51,105]. CEST was originally developed as a contrast mechanism in magnetic resonance imaging [106] and subsequently adapted to high resolution solution NMR spectroscopy [107]. In both CEST and DEST, the intensity of the resonance signal from the major chemical species is measured during application of a weak rf field. The frequency of the rf field is varied across the spectrum in separate experiments and the (normalized) intensity of the resonance plotted as a function of resonance offset. The experiments utilize the effects on the observed signal when the rf field is close to resonance with the unobservable sparsely populated state(s). The experiments differ primarily in that the CEST experiment relies on conventional exchange broadening by the variation in chemical shift between the major and minor states, while the DEST experiment relies on the difference in transverse relaxation rate constants between rapidly and slowly tumbling species in solution, typically a monomeric protein and a very large assemblage, such as an amyloid fibril.

A pulse sequence for the ^{15}N CEST/DEST experiment is shown in Fig. 10 [103]. The experiment is essentially a ^{15}N R_1 relaxation measurement with the addition of the weak rf field applied to the ^{15}N spins during the relaxation delay, *T*. The resulting profiles of *I*(*T*)/*I*(0) as a function of resonance offset are analyzed numerically using Eqs. (2)-(4) with $\boldsymbol{\rho}_k\,(t)=[\,M_{kx}\,(t), M_{ky}\,(t), M_{kz}\,(t)-p_k\,M_z^{eq}]$,

$$\mathbf{K}=\begin{bmatrix} -k_{12} & k_{21} \\ k_{12} & -k_{21} \end{bmatrix} - i\boldsymbol{L}_k - \hat{\boldsymbol{\Gamma}}_k = \begin{bmatrix} -R_{1k} & -\Omega_k & \omega_1 \\ \Omega_k & -R_{2k} & 0 \\ -\omega_1 & 0 & -R_{2k} \end{bmatrix} \quad (10)$$

and M_z^{eq} is the total equilibrium magnetization. Both CEST and DEST experiments are conventionally described as saturation transfer methods: when resonant with the sparsely populated states, the weak rf field saturates the minor state magnetization and the exchange kinetics transfer this saturation to the magnetization of spins in the major state. Many experiments in NMR spectroscopy can be usefully regarded from multiple theoretical perspectives. In this instance, both experiments can be treated as off-resonance $R_{1\rho}$ experiments to obtain insight into the expected results. For the CEST experiment, provided that $\Delta R_2^0=|R_{22}^0-R_{21}^0| \ll k_{ex}=k_{12}+k_{21}$ the expected rate constant is given by Eqs. (7) and (8). Baldwin and Kay have extended the results of Eqs. (7) and (8) to the situation in which $|\Delta R_2^0|>0$ [49]; the perturbation approach of Trott and Palmer [23] also can be extended to $|\Delta R_2^0|>0$ and yields a simpler expression (but slightly less accurate as p_2 increases):

NIH-PA Author Manuscript

NIH-PA Author Manuscript

NIH-PA Author Manuscript

$$R_{ex}=k_{12}\frac{\left\{\Delta\omega^2+(\Delta R_2^0)^2\right\}\ k_{21}+\Delta R_2^0(\omega_{1,eff}^2+k_{21}^2)}{k_{21}\ \left\{\omega_{2,eff}^2+k_{21}^2+(\Delta R_2^0)^2\right\}+\Delta R_2^0\omega_1^2} \quad (11)$$

If $\omega_1 \to 0$ and $\Omega_1 \to 0$, then Eq. (10) reduces to Eq. (5) and if $\Delta R_2^0 \to 0$and $p_b \to 0$, then Eq. (10) reduces to Eqs. (7) and (8). As already noted, the perturbation approach also can be applied to obtain relaxation rate constants for *N*-site exchange. The observed signal in the CEST or DEST experiments is approximately:

$$I(T)/I(0)=cos^2\theta\, exp(-T\ \cdot\ R_{1\rho}) \quad (12)$$

in which the factor of $\cos^2\theta$results from projection of the longitudinal magnetization onto the tilted reference frame (this factor rapidly approaches unity for weak rf fields off-resonance with respect to the population-average chemical shift). This analysis does not consider the contribution near resonance from evolution of magnetization components orthogonal to the tilted *z*-axis; for long irradiation times used in CEST and DEST experiments, these components dephase owing to $R_{2\rho}$ relaxation and ω_1 inhomogeneity. Sample calculations are shown in Fig. 11 for a system with similar kinetic parameters, but $\Delta R_2^0=0$ for application of the CEST experiment and $\Delta R_2^0 \gg 0$ for application of the DEST experiment. An additional calculation shows the result of $\Delta R_2^0>0$ in the CEST experiment. In this latter case, the width of the $I(T)/I(0)$ curve at the position of the minor resonance is broadened; as the value of ΔR_2^0 becomes larger and larger, this peak merges into the central peak and CEST becomes equivalent to DEST. The agreement between the exact calculation and the $R_{1\rho}$ approximation is excellent for both experiments. Thus, a viewpoint is established that provides unified insights into CEST, DEST, and conventional $R_{1\rho}$ experiments over the full range of spin-locking amplitudes.

7. Applications to nucleic acids

The above chemical exchange methods developed and applied to proteins have analogues adapted for applications to DNA and RNA nucleic acid molecules; such approaches have been reviewed recently [108] and are only described in brief herein. In contrast to proteins, nucleic acids have more sparsely distributed ^{15}N spins suitable as probes of chemical exchange, notably the imino nitrogen sites of G and T/U nucleobases. Rapid solvent exchange of imino hydrogens can reduce the sensitivity and accuracy of relaxation measurements, particularly for solvent-exposed conformational states. Thus, to circumvent these concerns, an early application to the lead-dependent ribozyme utilized ^{13}C $R_{1\rho}$ measurements for the isolated C2 sites of A and C8 sites of A and G nucleobases in uniformly ^{13}C/^{15}N enriched molecules [109]. The authors noted the potential difficulties posed by ^{13}C–^{13}C scalar and dipolar interactions for C6 of pyrimidines and other ^{13}C sites in fully labeled RNA molecules. As for proteins, isotopic labeling strategies have been developed to increase the number of isolated ^{13}C spins suitable for relaxation dispersion and other relaxation measurements [110-112]. Selective excitation and decoupling schemes can be used to minimize complications of ^{13}C–^{13}C interactions in natural abundance and isotopically enriched molecules [113]. The ^{1}H–^{1}H dipole–dipole interactions of imino ^{1}H

NIH-PA Author Manuscript

NIH-PA Author Manuscript

NIH-PA Author Manuscript

spins can be suppressed approximately by pulse sequence elements that average ROE and NOE interactions in $^{1}H–^{1}H$ ZZ-exchange experiments [114]. Applications of chemical exchange methods to nucleic acids have revealed a host of intramolecular dynamic processes, including loop repacking and rearrangement of secondary structures [108,109]. In notable applications, ^{13}C ZZ-exchange or relaxation dispersion methods have been used to characterize transitions between Watson–Crick and Hoogsteen base pairing in DNA oligonucleotides [115,116] and folding equilibria of “bistable” RNA oligonucleotides [117].

8. Computational methods

Computational methods, such as molecular dynamics simulations, have long been used in conjunction with NMR spin relaxation studies of conformational dynamics on ps–ns time scales [118-121]. The continued growth in computational power and methods has begun to have similar impact on NMR investigations of chemical exchange in at least three areas: generation of structural models that may represent minor chemical states, calculation of structures of minor species from chemical shifts and other NMR-observables extracted from relaxation dispersion studies, and direct simulation of chemical exchange processes.

In the first area, structural models have been generated from many approaches, including hand-building hypothetical structures [122], extraction of frames from molecular dynamics (MD) simulations [123], and computation of ensembles of structures using other experimental data, such as residual dipole couplings [85,124]. These approaches might be described as “forward methods”: the structural models are validated or selected by comparing values of $\Delta\omega$ (for slow exchange) or $p_1p_2\,\Delta\omega 2$ (for fast exchange) calculated from the models to experimental data. The second approach is an “inverse method”: given the experimental data, structural models are calculated using the experimental data as restraints on the structure determination algorithm [125]. The first example used the CS-Rosetta program to determine the structure of a folding intermediate for the FF domain from HYPA/FBP11 [126]. The calculation used backbone ^{15}N, $^{1}H^{N}$, $^{13}C^{\alpha}$, $^{1}H^{\alpha}$, and ^{13}CO relaxation dispersion measurements at static field strengths of 11.7 T and 18.8 T to obtain chemical shifts and amide N–H RDCs of the intermediate. A similar protocol was used subsequently to determine the structure of sparsely populated state of the T4 lysozyme L99A mutant [127]. In an alternative approach [128], the structure of a sparsely populated equilibrium on-pathway folding intermediate of the A39V/N53P/V55L mutant of the Fyn SH3 domain was determined from relaxation dispersion data, including ^{15}N, $^{1}H^{N}$, ^{13}CO, $^{13}C\alpha$, and $^{1}H\alpha$ backbone chemical shifts; $^{15}N–^{1}H^{N}$ RDCs; and ^{13}CO residual chemical shift anisotropies, using restrained MD simulations and CamShift [125]. The C-terminal residues 57–59 are disordered in the intermediate, disrupting β-strand 5. Mutants lacking the C-terminal residues form fibrillar aggregates, suggesting that the intermediate is aggregation-prone and can initiate fibrillation. Importantly, in all three cases, the mutations designed from the calculated structures allow validation of these approaches by stabilizing or mimicking the sparsely populated states. As larger sets of chemical shifts become available from experiments such as CEST, direct calculations of the structures of sparsely populated chemical states will become routine and allow more structural insights into the properties and functions of rare conformations of biological macromolecules.

NIH-PA Author Manuscript

NIH-PA Author Manuscript

NIH-PA Author Manuscript

Parallel developments of powerful computer hardware and efficient simulation algorithms have extended the length of MD simulations from order 10^2 ps in the early 1990s to a few milliseconds (10^6 ps) at present. These simulation lengths begin to approach the values of $1/k_{ex}$ observed in relaxation dispersion studies and raise the prospect that relaxation dispersion results could be interpreted from simulations, in similar fashion as for faster time scale dynamic processes. In complete analogy to the calculation of time-correlation functions for the dipole–dipole interaction in conventional analyses of laboratory frame relaxation data, the time correlation function for chemical shifts is calculated by using SPARTA+ or other semi-empirical chemical shift computer program to obtain chemical shift values for individual frames of the MD trajectory. The Fourier transform of this correlation function is the spectral density function for the process and is directly related to the relaxation dispersion profile in the fast motional limit (in which a Redfield treatment applies) [129,130]:

$$R_{ex}=\omega_0^2\int_0^\infty \langle[\delta(t)-\overline{\delta}]\,[\delta(t+\tau)-\overline{\delta}]\rangle\, f(\tau)\,d\tau \quad (13)$$

in which ω_0 is the Larmor frequency, $\delta(t)$ is the calculated chemical shift (in ppm) at time t in the trajectory, angle brackets indicate averaging over the trajectory. The function $f(t) = 1$, $\cos(\omega_1 t)$, or $\mathrm{tri}[\pi t/(2\tau_{cp})]$ for free-precession, $R_{1\rho}$, or CPMG experiments, respectively, and $\mathrm{tri}(x)$ is the triangle wave with extreme values (0, 1), $(\pi, -1)$, $(2\pi, 1)$ *et cetera*.

The most detailed analyses to date have been based on a 1-ms simulation of BPTI [130,131]. Extensive experimental data exist for BPTI on the dynamics of disulfide bond isomerization [122,132], flipping of aromatic rings [133], and exchange of buried water molecules with bulk solvent [134]. Conformations consistent with experimental results are sampled in the simulation, but the statistical sampling of conformations in the simulation does not converge to the experimentally determined populations of the alternative states [130]. Thus, chemical exchange rate constants calculated from the trajectory are in qualitative, but not quantitative agreement with experiment. Additional conformations are observed in the MD simulations that have not been detected experimentally by relaxation dispersion methods. Amide hydrogen exchange in proteins reports on very small populations of conformations competent for exchange with solvent. Recent work has compared amide hydrogen exchange rates for BPTI with predictions from MD simulations and concluded that the populations of such novel conformations are likely overestimated by current computational methods [135]. In related work, the exchange of buried water molecules in BPTI with bulk solvent in the 1-ms simulation has been analyzed using a stochastic point process formalism [136]. Even a 1-ms simulation is short compared to the kinetic rate constants observed experimentally for BPTI, limiting statistical convergence of the MD analysis. However, inexorable advances in computer power (coupled with developments in force fields and water models) will continue to increase the synergy between NMR relaxation and MD simulations. Indeed, 1-ms MD simulations of the 76-residue protein ubiquitin have been reported recently [137].

9. Discussion

Investigations of conformational dynamics of biological macromolecules are germane particularly to three broad problems in biology: folding and other disorder–order transitions,

NIH-PA Author Manuscript

NIH-PA Author Manuscript

NIH-PA Author Manuscript

molecular recognition and oligomerization, and enzyme catalysis. Emerging themes in many of these applications are: (i) “allosteric pathways” composed of spatially adjacent moieties with similar conformational dynamical properties enable coupling between spatially distal regions of structure and (ii) conformational differences between higher-energy sparsely populated states and the major ground state species enable tuning and regulation of function [138-143]. Chemical exchange phenomena are convenient probes of aspects of each of these phenomena owing to a fortuitous matching between the kinetic time scales of these processes and the (ever-increasing) time scales accessible to NMR experiments as well as to the exquisite sensitivity of the chemical shift (and dipole coupling constants) to chemical environment. Experimental developments in the recent past and foreseeable future provide both access to novel chemical systems, such as the DEST method for monomer-fibril exchange [51] or methyl-TROSY techniques for very large molecular machines [100], and increased accuracy of existing methods [82], allowing ever-finer dissection of dynamic contributions to function. A testament of the power of NMR spin relaxation methods and the subtlety of biological macromolecules is that nearly every application to a novel system reveals some unexpected feature linking conformational flexibility and dynamics to function.

Exchange methods have been used to measure ultra-fast protein folding rates that are otherwise difficult to access experimentally [144]. Relaxation dispersion measurements also allow folding rates to be measured at equilibrium under native-like conditions. These measurements are then important controls for other techniques that require perturbation with denaturant. Relaxation dispersion methods also have been used (*vide supra*) to characterize sparsely populated conformational states in solution that may represent (on- or off-pathway) folding intermediates [96,104,126,145]. Relaxation dispersion results for wild-type and mutant proteins can be used for φ-value analysis [146,147]. The NMR φ-value approach has the advantage over more usual methods, such as fluorescence spectroscopy, in that confounding structural perturbations caused by mutation can be identified by examination of chemical shift changes between wild-type and mutant species.

In many applications of relaxation dispersion measurements, sparsely populated states of apo proteins are detected that resemble the conformations observed in complexes with other molecules or otherwise activated states [85,148]. These results naturally leads to the hypothesis that molecular recognition or activation is through a “selected-fit” or “population-shift” mechanism. However, as emphasized by a number of authors [29,149], induced-fit and selected-fit mechanisms both are likely to be feasible in particular systems and the flux through each pathway depends on the various rate constants for steps along each pathway. For example, the following scheme represents the selected-fit mechanism along the upper pathway and the induced-fit mechanism along the lower pathway for simple ligand binding:

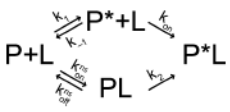

NIH-PA Author Manuscript

NIH-PA Author Manuscript

NIH-PA Author Manuscript

in which P and P* are ground-state (binding-incompetent) and activated-state (binding-competent) conformations of the protein, PL is a non-specific encounter complex, and P * L is the final complex. The relative flux through each pathway, when the initial concentration of P * L is negligible, is given by [29]:

$$F = \left(\frac{k_2\, k_{ns}^{on}}{k_1\, k_{on}}\right)\left(\frac{k_{-1}+k_{on}\,[L]}{k_2+k_{off}^{ns}}\right) = \left(\frac{K}{K_{ns}}\right)\left(\frac{k_2}{k_{on}\,[L]}\right) \quad (14)$$

and $K = (k_{-1} + k_{on}[L])/k_1$ and $K_{ns}=(k_2+k_{off}^{ns})/(k_{off}^{ns}\,[L])$. Full characterization of interaction mechanisms thus requires characterization of all the kinetic rate constants in the proposed mechanistic scheme, a goal that no doubt will spur additional experimental developments as well as joint investigations coupling NMR methods with other biophysical computational and experimental approaches. Furthermore, more complex, multi-step interaction mechanisms, such as coupled folding and binding [150], share aspects of both selected- and induced-fit recognition. Intramolecular interactions that compete with intermolecular ones are recognized increasingly as important for autoinhibition and modulation of affinity [151,152]. Investigations by chemical exchange methods have provided insight into the role of transient fluctuations to “activated” states in these processes.

The investigation of enzyme catalysis naturally bifurcates into two areas: contributions to the chemical step of catalysis and contributions to other aspects of enzyme function, including, substrate and cofactor binding, product release, and regulation of activity. Aspects of the latter category involve molecular interactions that share features with investigations of molecular recognition; consequently many of the same experimental approaches and interpretive schemes are utilized. A major insight, emerging from studies of DHFR, is that conformational fluctuations can poise an enzyme to bind the next substrate or cofactor in a multi-step enzymatic cycle [140,153]. The controversy in this area revolves around whether conformational dynamics observable by NMR spectroscopy [154-156] contribute to the rate of the chemical step, i.e. exert an effect on k_{cat} [157]. An experimental difficulty is that mutations, or other perturbations, that alter conformational dynamics (transitions over the energetic barriers relevant to the conformational change) also may alter subtly the (distinct) activation barrier controlling the chemical step. As discussed theoretically, molecular motions on a free-energy surface do not alter the surface, but could contribute to prefactors (entropic barriers or effective diffusion constants) in models for chemical kinetics [158,159]. Relaxation dispersion methods now are being applied to an ever-increasing number of enzymes; the resulting NMR data, combined with computational methods, promises to resolve long-standing questions in enzyme biophysics.

An important question that arises in all investigations of chemical exchange broadening is how many chemical states are kinetically coupled. Most of the analyses discussed above have assumed two-state-like behavior. Three-state exchange has been identified in a number of systems [122,145,146]. Variation of the sample temperature (or other relevant experimental parameter) alters the relative contribution of the exchange processes to the observed relaxation dispersion data and facilitates dissection of multi-step pathways. The CEST experiment (the weak field $R_{1\rho}$ limit) can distinguish in favorable cases between two- and three-state exchange [23,103]. Resolution of kinetic parameters for four-state exchange

NIH-PA Author Manuscript

NIH-PA Author Manuscript

NIH-PA Author Manuscript

mechanisms is likely to require additional constraints on fitting parameters from other biophysical or biochemical experiments [160]. As a simplification, theoretical analyses of free-precession and $R_{1\rho}$ relaxation rate constants illustrate that rapid averaging within a subset of sites reduces an *N*-site problem to exchange between a smaller number of "effective" states [23]. For example, investigations of folding implicitly assume that "random-coil" conformations are exchanging between allowed regions of conformational space on time scales faster than can be resolved by relaxation dispersion methods. As evident from long MD simulations [130,131], additional states not yet detected by NMR relaxation dispersion methods may exist and be functional. Increased precision and accuracy of experimental methods promises to allow detection of additional and even rarer conformational states of biological macromolecules.

10. Conclusion

Detailed investigations of sparsely populated chemical or conformational states of proteins and nucleic acids have established the power of relaxation dispersion and other chemical exchange techniques in NMR spectroscopy. Global analysis of data from multiple nuclear spin types, multiple magnetic fields, and multiple techniques improves the reliability of fitted kinetic model parameters; however, efficiency, that is minimizing total NMR acquisition time while maximizing sensitivity and accuracy, is critically important for applications of NMR spectroscopy to biological macromolecules, which may have limited solubilities and stabilities under NMR-suitable conditions. The pace of development of new techniques is likely to continue unabated and progress can be anticipated in experimental design to optimize information content and efficiency. Fundamental insights have been obtained into the functional roles of conformations other than ground state structures, and often populated at only a few percent in solution, in folding, recognition, and catalysis by biological macromolecules. In all likelihood, only a small number of possible biological mechanisms utilizing the properties of these alternative states have been described so far. Unanticipated insights no doubt will emerge from applications to ever more complex biological systems. If "past is prologue" (*The Tempest*), then the future is bright for chemical exchange investigations of function of biological macromolecules.

Acknowledgments

Support from NIH Grant GM59273 is acknowledged gratefully. I thank Drs. Michelle Gill, Ying Li, Paul Robustelli (Columbia University) and Mark Rance (University of Cincinnati) for helpful discussions.

References

1. Cavanagh, J.; Fairbrother, WJ.; Palmer, AG.; Rance, M.; Skelton, NJ. Protein NMR Spectroscopy: Principles and Practice. second ed. Academic Press; San Diego, CA: 2007.
2. Forsén S, Hoffman RA. Study of moderately rapid chemical exchange reactions by means of nuclear magnetic double resonance. J Chem Phys. 1963; 39:2892.
3. Gutowsky HS, Saika A. Dissociation, chemical exchange, and the proton magnetic resonance in some aqueous electrolytes. J Chem Phys. 1953; 21:1688–1694.
4. Fejzo J, Westler WM, Macura S, Markley JL. Elimination of cross-relaxation effects from two-dimensional chemical-exchange spectra of macromolecules. J Am Chem Soc. 1990; 112:2574–2577.

NIH-PA Author Manuscript

NIH-PA Author Manuscript

NIH-PA Author Manuscript

5. Palmer AG, Rance M, Wright PE. Intramolecular motions of a zinc finger DNA-binding domain from xfin characterized by proton-detected natural abundance ^{13}C heteronuclear NMR spectroscopy. J Am Chem Soc. 1991; 113:4371–4380.
6. Kay LE, Torchia DA, Bax A. Backbone dynamics of proteins as studied by ^{15}N inverse detected heteronuclear NMR spectroscopy: application to staphylococcal nuclease. Biochemistry. 1989; 28:8972–8979. [PubMed: 2690953]
7. Palmer AG, Kroenke CD, Loria JP. Nuclear magnetic resonance methods for quantifying microsecond-to-millisecond motions in biological macromolecules. Methods Enzymol. 2001; 339:204–238. [PubMed: 11462813]
8. Massi F, Wang C, Palmer AG. Solution NMR and computer simulation studies of active site loop motion in triosephosphate isomerase. Biochemistry. 2006; 45:10787–10794. [PubMed: 16953564]
9. Hodsdon ME, Cistola DP. Ligand binding alters the backbone mobility of intestinal fatty acid-binding protein as monitored by ^{15}N NMR relaxation and ^{1}H exchange. Biochemistry. 1997; 36:2278–2290. [PubMed: 9047330]
10. Wang C, Karpowich N, Hunt JF, Rance M, Palmer AG. Dynamics of ATP-binding cassette contribute to allosteric control, nucleotide binding and energy tranduction in ABC transporters. J Mol Biol. 2004; 342:525–537. [PubMed: 15327952]
11. Akke M, Skelton NJ, Kördel J, Palmer AG, Chazin WJ. Effects of ion binding on the backbone dynamics in calbindin D_{9k} determined by ^{15}N NMR relaxation. Biochemistry. 1993; 32:9832–9843. [PubMed: 8373781]
12. Loria JP, Rance M, Palmer AG. A relaxation-compensated Carr–Purcell–Meiboom–Gill sequence for characterizing chemical exchange by NMR spectroscopy. J Am Chem Soc. 1999; 121:2331–2332.
13. Szyperski T, Luginbühl P, Otting G, Güntert P, Wüthrich K. Protein dynamics studied by rotating frame ^{15}N spin relaxation times. J Biomol NMR. 1993; 3:151–164. [PubMed: 7682879]
14. Akke M, Palmer AG. Monitoring macromolecular motions on microsecond to millisecond time scales by $R_{1\rho}$–R_1 constant relaxation time NMR spectroscopy. J Am Chem Soc. 1996; 118:911–912.
15. Otten R, Villali J, Kern D, Mulder FAA. Probing microsecond time scale dynamics in proteins by methyl ^{1}H Carr–Purcell–Meiboom–Gill relaxation dispersion NMR measurements: application to activation of the signaling protein NtrCr. J Am Chem Soc. 2010; 132:17004–17014. [PubMed: 21058670]
16. Baldwin AJ, Religa TL, Hansen DF, Bouvignies G, Kay LE. $^{13}CHD_2$ methyl group probes of millisecond time scale exchange in proteins by ^{1}H relaxation dispersion: an application to proteasome gating residue dynamics. J Am Chem Soc. 2010; 132:10992–10995. [PubMed: 20698653]
17. Weininger U, Liu Z, McIntyre DD, Vogel HJ, Akke M. Specific $^{12}C^{\beta}D_2{}^{12}C^{\gamma}D_2S^{13}C^{\varepsilon}HD_2$ isotopomer labeling of methionine to characterize protein dynamics by ^{1}H and ^{13}C NMR relaxation dispersion. J Am Chem Soc. 2012; 134:18562–18565. [PubMed: 23106551]
18. Hansen AL, Lundstrom P, Velyvis A, Kay LE. Quantifying millisecond exchange dynamics in proteins by CPMG relaxation dispersion NMR using side-chain ^{1}H probes. J Am Chem Soc. 2012; 134:3178–3189. [PubMed: 22300166]
19. Krushelnitsky A, Reichert D, Saalwachter K. Solid-state NMR approaches to internal dynamics of proteins: from picoseconds to microseconds and seconds. Acc Chem Res. 2013; 46:2028–2036. [PubMed: 23875699]
20. Abergel D, Palmer AG. On the use of the stochastic Liouville equation in NMR: application to $R_{1\rho}$ relaxation in the presence of exchange. Concepts Magn Reson A. 2003; 19:134–148.
21. Sugase K, Konuma T, Lansing JC, Wright PE. Fast and accurate fitting of relaxation dispersion data using the flexible software package GLOVE. J Biomol NMR. 2013; 56:275–283. [PubMed: 23754491]
22. Bieri M, Gooley PR. Automated NMR relaxation dispersion data analysis using NESSY. BMC Bioinformatics. 2011; 12:421. [PubMed: 22032230]

NIH-PA Author Manuscript

NIH-PA Author Manuscript

NIH-PA Author Manuscript

23. Trott O, Palmer AG. Theoretical study of $R_{1\rho}$ rotating-frame and R_2 free-precession relaxation in the presence of n-site chemical exchange. J Magn Reson. 2004; 170:104–112. [PubMed: 15324763]
24. Jeener J, Meier BH, Bachmann P, Ernst RR. Investigation of exchange processes by two-dimensional NMR spectroscopy. J Chem Phys. 1979; 71:4546–4553.
25. Montelione GT, Wagner G. 2D chemical exchange NMR spectroscopy by proton-detected heteronuclear correlation. J Am Chem Soc. 1989; 111:3096–3098.
26. Wider G, Neri D, Wüthrich K. Studies of slow conformational equilibria in macromolecules by exchange of heteronuclear longitudinal 2-spin-order in a 2D difference correlation experiment. J Biomol NMR. 1991; 1:93–98.
27. Farrow N, Zhang O, Forman-Kay JD, Kay LE. A heteronuclear correlation experiment for simultaneous determination of ^{15}N longitudinal decay and chemical exchange rates of systems in slow equilibrium. J Biomol NMR. 1994; 4:727–734. [PubMed: 7919956]
28. Li Y, Altorelli NL, Bahna F, Honig B, Shapiro L, Palmer AG. Mechanism of E-cadherin dimerization probed by NMR relaxation dispersion. Proc Natl Acad Sci U S A. 2013; 110:16462–16467. [PubMed: 24067646]
29. Miloushev VZ, Bahna F, Ciatto C, Ahlsen G, Honig B, Shapiro L, Palmer AG. Dynamic properties of a type II cadherin adhesive domain: implications for the mechanism of strand-swapping of classical cadherins. Structure. 2008; 16:1195–1205. [PubMed: 18682221]
30. Hu K, Westler WM, Markley JL. Simultaneous quantification and identification of individual chemicals in metabolite mixtures by two-dimensional extrapolated time-zero $^{1}H–^{13}C$ HSQC (HSQC(0)). J Am Chem Soc. 2011; 133:1662–1665. [PubMed: 21247157]
31. Li Y, Palmer AG. TROSY-selected ZZ-exchange experiment for characterizing slow chemical exchange in large proteins. J Biomol NMR. 2009; 45:357–360. [PubMed: 19890725]
32. Sahu D, Clore GM, Iwahara J. TROSY-based z-exchange spectroscopy: application to the determination of the activation energy for intermolecular protein translocation between specific sites on different DNA molecules. J Am Chem Soc. 2007; 129:13232–13237. [PubMed: 17918842]
33. Palmer AG, Grey MJ, Wang C. Solution NMR spin relaxation methods for characterizing chemical exchange in high-molecular-weight systems. Methods Enzymol. 2005; 394:430–465. [PubMed: 15808232]
34. Morrison EA, DeKoster GT, Dutta S, Vafabakhsh R, Clarkson MW, Bahl A, Kern D, Ha T, Henzler-Wildman KA. Antiparallel EmrE exports drugs by exchanging between asymmetric structures. Nature. 2012; 481:45–50. [PubMed: 22178925]
35. Wang H, He Y, Kroenke CD, Kodukula S, Storch J, Palmer AG, Stark RE. Titration and exchange studies of liver fatty acid-binding protein with ^{13}C-labeled long-chain fatty acids. Biochemistry. 2002; 41:5453–5461. [PubMed: 11969406]
36. Igumenova TI, Brath U, Akke M, Palmer AG. Characterization of chemical exchange using residual dipolar coupling. J Am Chem Soc. 2007; 129:13396–13397. [PubMed: 17929930]
37. Vallurupalli P, Hansen DF, Stollar E, Meirovitch E, Kay LE. Measurement of bond vector orientations in invisible excited states of proteins. Proc Natl Acad Sci U S A. 2007; 104:18473–18477. [PubMed: 18006656]
38. Sarkar R, Vasos PR, Bodenhausen G. Singlet-state exchange NMR spectroscopy for the study of very slow dynamic processes. J Am Chem Soc. 2007; 129:328–334. [PubMed: 17212412]
39. Davis DG, Perlman ME, London RE. Direct measurements of the dissociation-rate constant for inhibitor-enzyme complexes via the $T_{1\rho}$ and T_2 (CPMG) methods. J Magn Reson Ser B. 1994; 104:266–275. [PubMed: 8069484]
40. Traaseth NJ, Chao F-A, Masterson LR, Mangia S, Garwood M, Michaeli S, Seelig B, Veglia G. Heteronuclear adiabatic relaxation dispersion (HARD) for quantitative analysis of conformational dynamics in proteins. J Magn Reson. 2012; 219:75–82. [PubMed: 22621977]
41. Mangia S, Traaseth NJ, Veglia G, Garwood M, Michaeli S. Probing slow protein dynamics by adiabatic $R_{1\rho}$ and $R_{2\rho}$ NMR experiments. J Am Chem Soc. 2010; 132:9979–9981. [PubMed: 20590094]

NIH-PA Author Manuscript

NIH-PA Author Manuscript

NIH-PA Author Manuscript

42. Carver JP, Richards RE. A general two-site solution for the chemical exchange produced dependence of T_2 upon the Carr–Purcell pulse separation. J Magn Reson. 1972; 6:89–105.
43. Allerhand A, Thiele E. Analysis of Carr–Purcell spin-echo NMR experiments on multiple-spin systems. II. The effect of chemical exchange. J Chem Phys. 1966; 45:902–916.
44. Jen J. Chemical exchange and NMR T_2 relaxation—the multisite case. J Magn Reson. 1978; 30:111–128.
45. Ishima R, Torchia DA. Estimating the time scale of chemical exchange of proteins from measurements of transverse relaxation rates in solution. J Biomol NMR. 1999; 14:369–372. [PubMed: 10526408]
46. Trott O, Palmer AG. $R_{1\rho}$ relaxation outside of the fast-exchange limit. J Magn Reson. 2002; 154:157–160. [PubMed: 11820837]
47. Trott O, Abergel D, Palmer AG. An average-magnetization analysis of $R_{1\rho}$ relaxation outside of the fast exchange. Mol Phys. 2003; 101:753–763.
48. Miloushev VZ, Palmer AG. $R_{1\rho}$ relaxation for two-site chemical exchange: general approximations and some exact solutions. J Magn Reson. 2005; 177:221–227. [PubMed: 16143548]
49. Baldwin AJ, Kay LE. An $R_{1\rho}$ expression for a spin in chemical exchange between two sites with unequal transverse relaxation rates. J Biomol NMR. 2013; 55:211–218. [PubMed: 23340732]
50. Ishima R, Torchia DA. Accuracy of optimized chemical-exchange parameters derived by fitting CPMG R_2 dispersion profiles when R20a≠R20b. J Biomol NMR. 2006; 34
51. Fawzi NL, Ying J, Ghirlando R, Torchia DA, Clore GM. Atomic-resolution dynamics on the surface of amyloid-β protofibrils probed by solution NMR. Nature. 2011; 480:268–272. [PubMed: 22037310]
52. Skrynnikov NR, Dahlquist FW, Kay LE. Reconstructing NMR spectra of “invisible” excited protein states using HSQC and HMQC experiments. J Am Chem Soc. 2002; 124:12352–12360. [PubMed: 12371879]
53. Auer R, Hansen DF, Neudecker P, Korzhnev DM, Muhandiram DR, Konrat R, Kay LE. Measurement of signs of chemical shift differences between ground and excited protein states: a comparison between H(S/M)QC and $R_{1\rho}$ methods. J Biomol NMR. 2010; 46:205–216. [PubMed: 20033258]
54. Baldwin AJ, Kay LE. Measurement of the signs of methyl ^{13}C chemical shift differences between interconverting ground and excited protein states by $R_{1\rho}$: an application to αB-crystallin. J Biomol NMR. 2012; 53:1–12. [PubMed: 22476760]
55. Palmer AG, Skelton NJ, Chazin WJ, Wright PE, Rance M. Suppression of the effects of cross-correlation between dipolar and anisotropic chemical shift relaxation mechanisms in the measurement of spin-spin relaxation rates. Mol Phys. 1992; 75:699–711.
56. Mulder FAA, Skrynnikov NR, Hon B, Dahlquist FW, Kay LE. Measurement of slow (μs-ms) time scale dynamics in protein side chains by ^{15}N relaxation dispersion NMR spectroscopy: application to Asn and Gln residues in a cavity mutant of T4 lysozyme. J Am Chem Soc. 2001; 123:967–975. [PubMed: 11456632]
57. Skrynnikov NR, Mulder FAA, Hon B, Dahlquist FW, Kay LE. Probing slow time scale dynamics at methyl-containing side chains in proteins by relaxation dispersion NMR measurements: application to methionine residues in a cavity mutant of T4 lysozyme. J Am Chem Soc. 2001; 123:4556–4566. [PubMed: 11457242]
58. Hansen DF, Vallurupalli P, Kay LE. An improved ^{15}N relaxation dispersion experiment for the measurement of millisecond time-scale dynamics in proteins. J Phys Chem B. 2008; 112:5898–5904. [PubMed: 18001083]
59. Esadze A, Li D-W, Wang T-Z, Brüschweiler R, Iwahara J-J. Dynamics of lysine side-chain amino groups in a protein studied by heteronuclear $^{1}H–^{15}N$ NMR spectroscopy. J Am Chem Soc. 2011; 133:909–919. [PubMed: 21186799]
60. Korzhnev DM, Skrynnikov NR, Millet O, Torchia DA, Kay LE. An NMR experiment for the accurate measurement of heteronuclear spin-lock relaxation rates. J Am Chem Soc. 2002; 124:10743–10753. [PubMed: 12207529]

NIH-PA Author Manuscript NIH-PA Author Manuscript NIH-PA Author Manuscript

61. Massi F, Johnson E, Wang CY, Rance M, Palmer AG. NMR $R_{1\rho}$ rotating-frame relaxation with weak radio frequency fields. J Am Chem Soc. 2004; 126:2247–2256. [PubMed: 14971961]
62. Ban D, Gossert AD, Giller K, Becker S, Griesinger C, Lee D. Exceeding the limit of dynamics studies on biomolecules using high spin-lock field strengths with a cryogenically cooled probehead. J Magn Reson. 2012; 221:1–4. [PubMed: 22743535]
63. Kloiber K, Konrat R. Differential multiple-quantum relaxation arising from cross-correlated time-modulation of isotropic chemical shifts. J Biomol NMR. 2000; 18:33–42. [PubMed: 11061226]
64. Dittmer J, Bodenhausen G. Evidence for slow motion in proteins by multiple refocusing of heteronuclear nitrogen/proton multiple quantum coherences in NMR. J Am Chem Soc. 2004; 126:1314–1315. [PubMed: 14759169]
65. Korzhnev DM, Kloiber K, Kay LE. Multiple-quantum relaxation dispersion NMR spectroscopy probing millisecond time-scale dynamics in proteins: theory and application. J Am Chem Soc. 2004; 126:7320–7329. [PubMed: 15186169]
66. Lundström P, Akke M. Quantitative analysis of conformational exchange contributions to $^{1}H–^{15}N$ multiple-quantum relaxation using field-dependent measurements. Time scale and structural characterization of exchange in a calmodulin C-terminal domain mutant. J Am Chem Soc. 2004; 126:928–935. [PubMed: 14733570]
67. Orekhov VY, Korzhnev DM, Kay LE. Double- and zero-quantum NMR relaxation dispersion experiments sampling millisecond time scale dynamics in proteins. J Am Chem Soc. 2004; 126:1886–1891. [PubMed: 14871121]
68. Del Rio A, Anand A, Ghose R. Detection of correlated dynamics on multiple timescales by measurement of the differential relaxation of zero- and double-quantum coherences involving sidechain methyl groups in proteins. J Magn Reson. 2006; 180:1–17. [PubMed: 16473030]
69. Hansen DF, Yang D, Feng H, Zhou Z, Wiesner S, Bai Y, Kay LE. An exchange-free measure of ^{15}N transverse relaxation: an NMR spectroscopy application to the study of a folding intermediate with pervasive chemical exchange. J Am Chem Soc. 2007; 129:11468–11479. [PubMed: 17722922]
70. Gill ML, Palmer AG. Multiplet-filtered and gradient-selected zero-quantum TROSY experiments for $^{13}C^{1}H_3$ methyl groups in proteins. J Biomol NMR. 2011; 51:245–251. [PubMed: 21918814]
71. Salvi N, Ulzega S, Ferrage F, Bodenhausen G. Time scales of slow motions in ubiquitin explored by heteronuclear double resonance. J Am Chem Soc. 2012; 134:2481–2484. [PubMed: 22206505]
72. Majumdar A, Ghose R. Probing slow backbone dynamics in proteins using TROSY-based experiments to detect cross-correlated time-modulation of isotropic chemical shifts. J Biomol NMR. 2004; 28:213–227. [PubMed: 14752255]
73. Wang C, Palmer AG. Differential multiple quantum relaxation caused by chemical exchange outside the fast exchange limit. J Biomol NMR. 2002; 24:263–268. [PubMed: 12522313]
74. Millet O, Loria JP, Kroenke CD, Pons M, Palmer AG. The static magnetic field dependence of chemical exchange linebroadening defines the NMR chemical shift time scale. J Am Chem Soc. 2000; 122:2867–2877.
75. Wang CY, Grey MJ, Palmer AG. CPMG sequences with enhanced sensitivity to chemical exchange. J Biomol NMR. 2001; 21:361–366. [PubMed: 11824755]
76. Wang L, Pang Y, Holder T, Brender JR, Kurochkin AV, Zuiderweg ERP. Functional dynamics in the active site of the ribonuclease binase. Proc Natl Acad Sci U S A. 2001; 98:7684–7689. [PubMed: 11438724]
77. Wang CY, Rance M, Palmer AG. Mapping chemical exchange in proteins with MW > 50 kD. J Am Chem Soc. 2003; 125:8968–8969. [PubMed: 15369325]
78. Phan IQH, Boyd J, Campbell ID. Dynamic studies of a fibronectin type I module pair at three frequencies: anisotropic modeling and direct determination of conformational exchange. J Biomol NMR. 1996; 8:369–378. [PubMed: 20859776]
79. Kroenke CD, Loria JP, Lee LK, Rance M, Palmer AG. Longitudinal and transverse $^{1}H–^{15}N$ dipolar/^{15}N chemical shift anisotropy relaxation interference: unambiguous determination of rotational diffusion tensors and chemical exchange effects in biological macromolecules. J Am Chem Soc. 1998; 120:7905–7915.

NIH-PA Author Manuscript

NIH-PA Author Manuscript

NIH-PA Author Manuscript

80. Mulder FAA, van Tilborg PJA, Kaptein R, Boelens R. Microsecond time scale dynamics in the RXR DNA-binding domain from a combination of spin-echo and off-resonance rotating frame relaxation measurements. J Biomol NMR. 1999; 13:275–288. [PubMed: 10212986]
81. Ban D, Mazur A, Carneiro MG, Sabo TM, Giller K, Koharudin LM, Becker S, Gronenborn AM, Griesinger C, Lee D. Enhanced accuracy of kinetic information from CT-CPMG experiments by transverse rotating-frame spectroscopy. J Biomol NMR. 2013; 57:73–82. [PubMed: 23949308]
82. Lakomek NA, Ying J, Bax A. Measurement of ^{15}N relaxation rates in perdeuterated proteins by TROSY-based methods. J Biomol NMR. 2012; 53:209–221. [PubMed: 22689066]
83. Igumenova TI, Palmer AG. Off-resonance TROSY-selected $R_{1\rho}$ experiment with improved sensitivity for medium- and high-molecular-weight proteins. J Am Chem Soc. 2006; 128:8110–8111. [PubMed: 16787055]
84. Vallurupalli P, Hansen DF, Kay LE. Probing structure in invisible protein states with anisotropic NMR chemical shifts. J Am Chem Soc. 2008; 130:2734–2735. [PubMed: 18257570]
85. Ban D, Funk M, Gulich R, Egger D, Sabo TM, Walter KF, Fenwick RB, Giller K, Pichierri F, de Groot BL, Lange OF, Grubmuller H, Salvatella X, Wolf M, Loidl A, Kree R, Becker S, Lakomek NA, Lee D, Lunkenheimer P, Griesinger C. Kinetics of conformational sampling in ubiquitin. Angew Chem Int Ed Engl. 2011; 50:11437–11440. [PubMed: 22113802]
86. Massi F, Grey MJ, Palmer AG. Microsecond timescale backbone conformational dynamics in ubiquitin studied with NMR $R_{1\rho}$ relaxation experiments. Protein Sci. 2005; 14:735–742. [PubMed: 15722448]
87. Ishima R, Torchia DA. Extending the range of amide proton relaxation dispersion experiments in protein using a constant-time relaxation-compensated CPMG approach. J Biomol NMR. 2003; 25:243–248. [PubMed: 12652136]
88. Eichmuller C, Skrynnikov NR. A new amide proton $R_{1\rho}$ experiment permits accurate characterization of microsecond time-scale conformational exchange. J Biomol NMR. 2005; 32:281–293. [PubMed: 16211482]
89. Lundström P, Akke M. Off-resonance rotating-frame amide proton spin relaxation experiments measuring microsecond chemical exchange in proteins. J Biomol NMR. 2005; 32:163–173. [PubMed: 16034667]
90. Auer R, Neudecker P, Muhandiram DR, Lundström P, Hansen DF, Konrat R, Kay LE. Measuring the signs of ^{1}Hα chemical shift differences between ground and excited protein states by off-resonance spin-lock $R_{1\rho}$ NMR spectroscopy. J Am Chem Soc. 2009; 131:10832–10833. [PubMed: 19606858]
91. Lundström P, Hansen DF, Vallurupalli P, Kay LE. Accurate measurement of a proton chemical shifts of excited protein states by relaxation dispersion NMR spectroscopy. J Am Chem Soc. 2009; 131:1915–1926. [PubMed: 19152327]
92. Vallurupalli P, Hansen DF, Lundström P, Kay LE. CPMG relaxation dispersion NMR experiments measuring glycine ^{1}Hα and ^{13}Cα chemical shifts in the 'invisible' excited states of proteins. J Biomol NMR. 2009; 45:45–55. [PubMed: 19319480]
93. Lundström P, Hansen DF, Kay LE. Measurement of carbonyl chemical shifts of excited protein states by relaxation dispersion NMR spectroscopy: comparison between uniformly and selectively ^{13}C labeled samples. J Biomol NMR. 2008; 42:35–47. [PubMed: 18762869]
94. Hansen DF, Vallurupalli P, Lundström P, Neudecker P, Kay LE. Probing chemical shifts of invisible states of proteins with relaxation dispersion NMR spectroscopy: how well can we do? J Am Chem Soc. 2008; 130:2667–2675. [PubMed: 18237174]
95. Ishima R, Baber J, Louis JM, Torchia DA. Carbonyl carbon transverse relaxation dispersion measurements and ms-μs timescale motion in a protein hydrogen bond network. J Biomol NMR. 2004; 29:187–198. [PubMed: 15014232]
96. O'Connell NE, Grey MJ, Tang Y, Kosuri P, Miloushev VZ, Raleigh DP, Palmer AG. Partially folded equilibrium intermediate of the villin headpiece HP67 defined by ^{13}C relaxation dispersion. J Biomol NMR. 2009; 45:85–98. [PubMed: 19644656]
97. Lundström P, Lin H, Kay LE. Measuring ^{13}Cβ chemical shifts of invisible excited states in proteins by relaxation dispersion NMR spectroscopy. J Biomol NMR. 2009; 44:139–155. [PubMed: 19448976]

NIH-PA Author Manuscript

NIH-PA Author Manuscript

NIH-PA Author Manuscript

98. Weininger U, Respondek M, Akke M. Conformational exchange of aromatic side chains characterized by L-optimized TROSY-selected ^{13}C CPMG relaxation dispersion. J Biomol NMR. 2012; 54:9–14. [PubMed: 22833056]
99. Ishima R, Louis JM, Torchia DA. Optimized labeling of $^{13}CHD_2$ methyl isotopomers in perdeuterated proteins: potential advantages for ^{13}C relaxation studies of methyl dynamics of larger proteins. J Biomol NMR. 2001; 21:167–171. [PubMed: 11727980]
100. Korzhnev DM, Kloiber K, Kanelis V, Tugarinov V, Kay LE. Probing slow dynamics in high molecular weight proteins by methyl-TROSY NMR spectroscopy: application to a 723-residue enzyme. J Am Chem Soc. 2004; 126:3964–3973. [PubMed: 15038751]
101. Grey MJ, Tang YF, Alexov E, McKnight CJ, Raleigh DP, Palmer AG. Characterizing a partially folded intermediate of the villin headpiece domain under non-denaturing conditions: contribution of His41 to the pH-dependent stability of the N-terminal subdomain. J Mol Biol. 2006; 355:1078–1094. [PubMed: 16332376]
102. Bouvignies G, Kay LE. Measurement of proton chemical shifts in invisible states of slowly exchanging protein systems by chemical exchange saturation transfer. J Phys Chem B. 2012; 116:14311–14317. [PubMed: 23194058]
103. Vallurupalli P, Bouvignies G, Kay LE. Studying “invisible” excited protein states in slow exchange with a major state conformation. J Am Chem Soc. 2012; 134:8148–8161. [PubMed: 22554188]
104. Hansen AL, Bouvignies G, Kay LE. Probing slowly exchanging protein systems via $^{13}C\alpha$-CEST: monitoring folding of the Im7 protein. J Biomol NMR. 2013; 55:279–289. [PubMed: 23386228]
105. Fawzi NL, Ying J, Torchia DA, Clore GM. Probing exchange kinetics and atomic resolution dynamics in high-molecular-weight complexes using dark-state exchange saturation transfer NMR spectroscopy. Nat Protoc. 2012; 7:1523–1533. [PubMed: 22814391]
106. van Zijl PC, Yadav NN. Chemical exchange saturation transfer (CEST): what is in a name and what isn’t? Magn Reson Med. 2011; 65:927–948. [PubMed: 21337419]
107. Lauzon CB, van Zijl P, Stivers JT. Using the water signal to detect invisible exchanging protons in the catalytic triad of a serine protease. J Biomol NMR. 2011; 50:299–314. [PubMed: 21809183]
108. Al-Hashimi HM. NMR studies of nucleic acid dynamics. J Magn Reson. 2013; 237:191–204. [PubMed: 24149218]
109. Hoogstraten CG, Wank JR, Pardi A. Active site dynamics in the lead-dependent ribozyme. Biochemistry. 2000; 39:9951–9958. [PubMed: 10933815]
110. Johnson JE Jr, Hoogstraten CG. Extensive backbone dynamics in the GCAA RNA tetraloop analyzed using ^{13}C NMR spin relaxation and specific isotope labeling. J Am Chem Soc. 2008; 130:16757–16769. [PubMed: 19049467]
111. Wunderlich CH, Spitzer R, Santner T, Fauster K, Tollinger M, Kreutz C. Synthesis of (6-^{13}C)pyrimidine nucleotides as spin-labels for RNA dynamics. J Am Chem Soc. 2012; 134:7558–7569. [PubMed: 22489874]
112. Nikolova EN, Al-Hashimi HM. Preparation, resonance assignment, and preliminary dynamics characterization of residue specific $^{13}C/^{15}N$-labeled elongated DNA for the study of sequence-directed dynamics by NMR. J Biomol NMR. 2009; 45:9–16. [PubMed: 19636798]
113. Hansen AL, Nikolova EN, Casiano-Negroni A, Al-Hashimi HM. Extending the range of microsecond-to-millisecond chemical exchange detected in labeled and unlabeled nucleic acids by selective carbon $R_{1\rho}$ NMR spectroscopy. J Am Chem Soc. 2009; 131:3818–3819. [PubMed: 19243182]
114. Latham MP, Zimmermann GR, Pardi A. NMR chemical exchange as a probe for ligand-binding kinetics in a theophylline-binding RNA aptamer. J Am Chem Soc. 2009; 131:5052–5053. [PubMed: 19317486]
115. Nikolova EN, Kim E, Wise AA, O’Brien PJ, Andricioaei I, Al-Hashimi HM. Transient Hoogsteen base pairs in canonical duplex DNA. Nature. 2011; 470:498–U484. [PubMed: 21270796]

NIH-PA Author Manuscript

NIH-PA Author Manuscript

NIH-PA Author Manuscript

116. Nikolova EN, Gottardo FL, Al-Hashimi HM. Probing transient Hoogsteen hydrogen bonds in canonical duplex DNA using NMR relaxation dispersion and single-atom substitution. J Am Chem Soc. 2012; 134:3667–3670. [PubMed: 22309937]
117. Kloiber K, Spitzer R, Tollinger M, Konrat R, Kreutz C. Probing RNA dynamics via longitudinal exchange and CPMG relaxation dispersion NMR spectroscopy using a sensitive ^{13}C-methyl label. Nucleic Acids Res. 2011; 39:4340–4351. [PubMed: 21252295]
118. Palmer AG, Case DA. Molecular dynamics analysis of NMR relaxation in a zinc-finger peptide. J Am Chem Soc. 1992; 114:9059–9067.
119. Kordel J, Teleman O. Backbone dynamics of calbindin D_{9k}: comparison of molecular dynamics simulations and ^{15}N NMR relaxation measurements. J Am Chem Soc. 1992; 114:4934–4936.
120. Lipari G, Szabo A, Levy RM. Protein dynamics and NMR relaxation: comparison of simulations with experiment. Nature. 1982; 300:197–198.
121. Levy RM, Karplus M. Trajectory studies of NMR relaxation in flexible molecules. Adv Chem Ser. 1983; 204:445–468. Mol.-Based. Study Fluids.
122. Grey MJ, Wang CY, Palmer AG. Disulfide bond isomerization in basic pancreatic trypsin inhibitor: multisite chemical exchange quantified by CPMG relaxation dispersion and chemical shift modeling. J Am Chem Soc. 2003; 125:14324–14335. [PubMed: 14624581]
123. Stafford KA, Robustelli P, Palmer AG. Thermal adaptation of conformational dynamics in ribonuclease H. PLoS Comput Biol. 2013; 9:e1003218. [PubMed: 24098095]
124. De Simone A, Montalvao RW, Dobson CM, Vendruscolo M. Characterization of the interdomain motions in hen lysozyme using residual dipolar couplings as replica-averaged structural restraints in molecular dynamics simulations. Biochemistry. 2013; 52:6480–6486. [PubMed: 23941501]
125. Robustelli P, Kohlhoff K, Cavalli A, Vendruscolo M. Using NMR chemical shifts as structural restraints in molecular dynamics simulations of proteins. Structure. 2010; 18:923–933. [PubMed: 20696393]
126. Korzhnev DM, Religa TL, Banachewicz W, Fersht AR, Kay LE. A transient and low-populated protein-folding intermediate at atomic resolution. Science. 2010; 329:1312–1316. [PubMed: 20829478]
127. Bouvignies G, Vallurupalli P, Hansen DF, Correia BE, Lange O, Bah A, Vernon RM, Dahlquist FW, Baker D, Kay LE. Solution structure of a minor and transiently formed state of a T4 lysozyme mutant. Nature. 2011; 477:111–114. [PubMed: 21857680]
128. Neudecker P, Robustelli P, Cavalli A, Walsh P, Lundstrom P, Zarrine-Afsar A, Sharpe S, Vendruscolo M, Kay LE. Structure of an intermediate state in protein folding and aggregation. Science. 2012; 336:362–366. [PubMed: 22517863]
129. Abergel D, Palmer AG. A Markov model for relaxation and exchange in NMR spectroscopy. J Phys Chem B. 2005; 109:4837–4844. [PubMed: 16863137]
130. Xue Y, Ward JM, Yuwen T, Podkorytov IS, Skrynnikov NR. Microsecond time-scale conformational exchange in proteins: using long molecular dynamics trajectory to simulate NMR relaxation dispersion data. J Am Chem Soc. 2012; 134:2555–2562. [PubMed: 22206299]
131. Shaw DE, Maragakis P, Lindorff-Larsen K, Piana S, Dror RO, Eastwood MP, Bank JA, Jumper JM, Salmon JK, Shan Y, Wriggers W. Atomic-level characterization of the structural dynamics of proteins. Science. 2010; 330:341–346. [PubMed: 20947758]
132. Otting G, Liepinsh E, Wüthrich K. Disulfide bond isomerization in BPTI and BPTI(G36S): an NMR study of correlated mobility in proteins. Biochemistry. 1993; 32:3571–3582. [PubMed: 7682109]
133. Skalicky JJ, Mills JL, Sharma S, Szyperski T. Aromatic ring-flipping in supercooled water: implications for NMR-based structural biology of proteins. J Am Chem Soc. 2001; 123:388–397. [PubMed: 11456540]
134. Denisov VP, Peters J, Horlein HD, Halle B. Using buried water molecules to explore the energy landscape of proteins. Nat Struct Biol. 1996; 3:505–509. [PubMed: 8646535]
135. Hernandez G, Anderson JS, LeMaster DM. Experimentally assessing molecular dynamics sampling of the protein native state conformational distribution. Biophys Chem. 2012; 163–164:21–34.

NIH-PA Author Manuscript NIH-PA Author Manuscript NIH-PA Author Manuscript

136. Persson F, Halle B. Transient access to the protein interior: simulation versus NMR. J Am Chem Soc. 2013; 135:8735–8748. [PubMed: 23675835]

137. Piana S, Lindorff-Larsen K, Shaw DE. Atomic-level description of ubiquitin folding. Proc Natl Acad Sci U S A. 2013; 110:5915–5920. [PubMed: 23503848]

138. Farber PJ, Mittermaier A. Concerted dynamics link allosteric sites in the PBX homeodomain. J Mol Biol. 2011; 405:819–830. [PubMed: 21087615]

139. Petit CM, Zhang J, Sapienza PJ, Fuentes EJ, Lee AL. Hidden dynamic allostery in a PDZ domain. Proc Natl Acad Sci U S A. 2009; 106:18249–18254. [PubMed: 19828436]

140. Boehr DD, Schnell JR, McElheny D, Bae SH, Duggan BM, Benkovic SJ, Dyson HJ, Wright PE. A distal mutation perturbs dynamic amino acid networks in dihydrofolate reductase. Biochemistry. 2013; 52:4605–4619. [PubMed: 23758161]

141. Popovych N, Sun S, Ebright RH, Kalodimos CG. Dynamically driven protein allostery. Nat Struct Mol Biol. 2006; 13:831–838. [PubMed: 16906160]

142. Brüschweiler S, Schanda P, Kloiber K, Brutscher B, Kontaxis G, Konrat R, Tollinger M. Direct observation of the dynamic process underlying allosteric signal transmission. J Am Chem Soc. 2009; 131:3063–3068. [PubMed: 19203263]

143. Kleckner IR, Gollnick P, Foster MP. Mechanisms of allosteric gene regulation by NMR quantification of microsecond-millisecond protein dynamics. J Mol Biol. 2012; 415:372–381. [PubMed: 22115774]

144. Vugmeyster L, Kroenke CD, Picart F, Palmer AG, Raleigh DP. ^{15}N $R_{1\rho}$ measurements allow the determination of ultrafast protein folding rates. J Am Chem Soc. 2000; 122:5387–5388.

145. Meinhold DW, Wright PE. Measurement of protein unfolding/refolding kinetics and structural characterization of hidden intermediates by NMR relaxation dispersion. Proc Natl Acad Sci U S A. 2011; 108:9078–9083. [PubMed: 21562212]

146. Neudecker P, Zarrine-Afsar A, Davidson AR, Kay LE. ϕ-Value analysis of a three-state protein folding pathway by NMR relaxation dispersion spectroscopy. Proc Natl Acad Sci U S A. 2007; 104:15717–15722. [PubMed: 17898173]

147. Cho J-H, O'Connell N, Raleigh DP, Palmer AG. ϕ-Value analysis for ultrafast folding proteins by NMR relaxation dispersion. J Am Chem Soc. 2010; 132:450–451. [PubMed: 20028088]

148. Volkman BF, Lipson D, Wemmer DE, Kern D. Two-state allosteric behavior in a single-domain signaling protein. Science. 2001; 291:2429–2433. [PubMed: 11264542]

149. Hammes GG, Chang YC, Oas TG. Conformational selection or induced fit: a flux description of reaction mechanism. Proc Natl Acad Sci U S A. 2009; 106:13737–13741. [PubMed: 19666553]

150. Sugase K, Dyson HJ, Wright PE. Mechanism of coupled folding and binding of an intrinsically disordered protein. Nature. 2007; 447:1021–1025. [PubMed: 17522630]

151. Cho J-H, Muralidharan V, Vila-Perello M, Raleigh DP, Muir TW, Palmer AG. Tuning protein autoinhibition by domain destabilization. Nat Struct Mol Biol. 2011; 18:550–555. [PubMed: 21532593]

152. Tzeng S-R, Kalodimos CG. Allosteric inhibition through suppression of transient conformational states. Nat Chem Biol. 2013; 9:462–465. [PubMed: 23644478]

153. Boehr DD, McElheny D, Dyson HJ, Wright PE. Millisecond timescale fluctuations in dihydrofolate reductase are exquisitely sensitive to the bound ligands. Proc Natl Acad Sci U S A. 2010; 107:1373–1378. [PubMed: 20080605]

154. Bhabha G, Lee J, Ekiert DC, Gam J, Wilson IA, Dyson HJ, Benkovic SJ, Wright PE. A dynamic knockout reveals that conformational fluctuations influence the chemical step of enzyme catalysis. Science. 2011; 332:234–238. [PubMed: 21474759]

155. Eisenmesser EZ, Millet O, Labeikovsky W, Korzhnev DM, Wolf-Watz M, Bosco DA, Skalicky JJ, Kay LE, Kern D. Intrinsic dynamics of an enzyme underlies catalysis. Nature. 2005; 438:117–121. [PubMed: 16267559]

156. Labeikovsky W, Eisenmesser EZ, Bosco DA, Kern D. Structure and dynamics of Pin1 during catalysis by NMR. J Mol Biol. 2007; 367:1370–1381. [PubMed: 17316687]

157. Kamerlin SC, Warshel A. At the dawn of the 21st century: is dynamics the missing link for understanding enzyme catalysis? Proteins. 2010; 78:1339–1375. [PubMed: 20099310]

NIH-PA Author Manuscript

NIH-PA Author Manuscript

NIH-PA Author Manuscript

158. Doshi U, McGowan LC, Ladani ST, Hamelberg D. Resolving the complex role of enzyme conformational dynamics in catalytic function. Proc Natl Acad Sci U S A. 2012; 109:5699–5704. [PubMed: 22451902]

159. Adamczyk AJ, Cao J, Kamerlin SC, Warshel A. Catalysis by dihydrofolate reductase and other enzymes arises from electrostatic preorganization, not conformational motions. Proc Natl Acad Sci U S A. 2011; 108:14115–14120. [PubMed: 21831831]

160. Li P, Martins IR, Rosen MK. The feasibility of parameterizing four-state equilibria using relaxation dispersion measurements. J Biomol NMR. 2011; 51:57–70. [PubMed: 21947915]

161. Shaka AJ, Barker PB, Freeman R. Computer-optimized decoupling scheme for wideband applications and low-level operation. J Magn Reson. 1985; 64:547–552.

162. Marion D, Ikura M, Tschudin R, Bax A. Rapid recording of 2D NMR spectra without phase cycling. Application to the study of hydrogen exchange in proteins. J Magn Reson. 1989; 85:393–399.

163. Mulder FAA, de Graaf RA, Kaptein R, Boelens R. An off-resonance rotating frame relaxation experiment for the investigation of macromolecular dynamics using adiabatic rotations. J Magn Reson. 1998; 131:351–357. [PubMed: 9571112]

164. Kay LE, Keifer P, Saarinen T. Pure absorption gradient enhanced heteronuclear single quantum correlation spectroscopy with improved sensitivity. J Am Chem Soc. 1992; 114:10663–10665.

165. Shaka AJ, Keeler J, Frenkiel T, Freeman R. An improved sequence for broadband decoupling: WALTZ-16. J Magn Reson. 1983; 52:334–338.

NIH-PA Author Manuscript

NIH-PA Author Manuscript

NIH-PA Author Manuscript

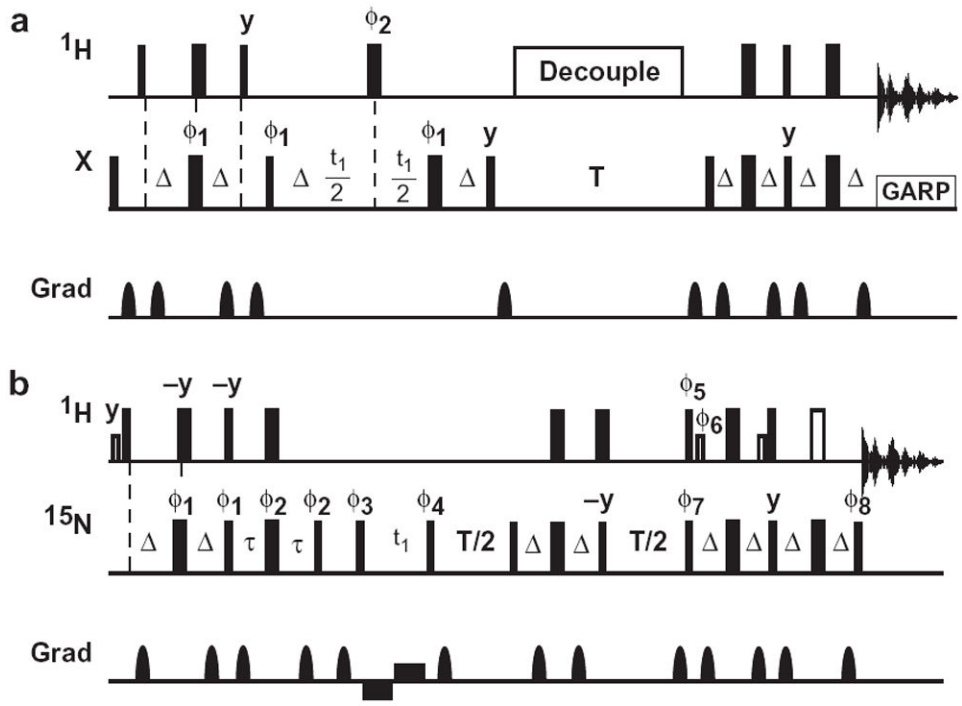

Fig. 1.

Pulse sequence diagrams for (a) in-phase HSQC-detected [27] and (b) ^{15}N TROSY-selected [31] ZZ-exchange experiments; the sequence in (a) is suitable for ^{13}C or ^{15}N spins (although water flip-back water suppression could be added in the case of ^{15}N spins in similar fashion as in (b)). Narrow and wide bars represent 90° and 180° pulses, respectively; short narrow open bars represent water-selective 90° pulses; and wide open bars represent crafted 180° pulses that leave the water magnetization unperturbed [1]. All pulse phases are *x* unless indicated otherwise. The delays are $\Delta = 1/(4J_{XH})$ and $\tau = 1/(8J_{XH})$. Gradients are used to suppress unwanted coherences and pulse imperfections. (a) Decoupling during the relaxation delay uses a train of ^{1}H 180° pulses. Decoupling during acquisition is achieved with the GARP sequence [161]. The phase cycle is $\varphi_1 = x, -x$; $\varphi_2 = x,x,y,y,-x,-x,-y,-y$; and receiver = $x,-x,-x,x$. Frequency discrimination is obtained by shifting the phase of the receiver and φ_1 according to the States-TPPI protocol [162]. (b) The phase cycle is $\varphi_1 = 4(x, -x,-y,y)$, $\varphi_2 = 2(135°,315°,45°,225°), 2(315°,135°,225°,45°)$, $\varphi_3 = 4(x,-x,-y,y)$, $\varphi_4 = 4(x, -x,y,-y)$, $\varphi_{5-5} = 2(y,y,y,y,-y,-y,-y,-y)$, $\varphi_6 = 2(-y,-y,-y,-y,y,y,y,y)$, $\varphi_7 = 4(-x,x,-y,y)$, $\varphi_8 = 2(x,x,x,x,-x,-x,-x,-x)$, $\varphi_{rec} = (x,-x,y,-y,x,-x,-y,y,-x,x,-y,y,-x,x,y,-y)$. Frequency discrimination is obtained by shifting the phase of the receiver and φ_4 according to the States-TPPI protocol [162].

NIH-PA Author Manuscript

NIH-PA Author Manuscript

NIH-PA Author Manuscript

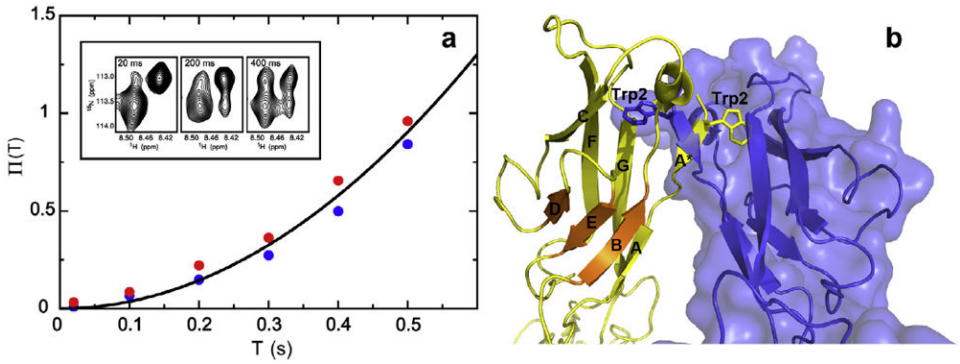

Fig. 2.

ZZ-exchange characterization of a monomer–dimer equilibrium for E-cadherin domains 1 and 2. (a) Composite peak intensity ratio Π(*T*) for ^{15}N ZZ-exchange measurements for residues Ile38 and Asp90 of a protein construct consisting of wild-type mouse E-cadherin extracellular domains 1 and 2 (EC1–EC2). The inset shows ^{15}N ZZ-exchange spectra of residue Ile38 at several mixing times. The solid lines are best-fits to the experimental data to a modification of Eq. (5) for a monomer–dimer equilibrium, yielding $k_{12} = k_{on} = (1.0 \pm 0.1) \times 10^4$ M^{-1} s^{-1} and $k_{21} = k_{off} = 0.8 \pm 0.1$ s^{-1} at 299 K. (b) Crystal structure of E-cadherin EC1–EC2 domains (Protein Data Bank (PDB) ID code 2qvf) showing the strand-swapped dimer interface of wild type protein. Reprinted from Y. Li, N. Altorelli, F. Bahna, B. Honig, L. Shapiro, A.G. Palmer, Mechanism of E-cadherin dimerization probed by NMR relaxation dispersion, Proc. Natl. Acad. Sci. USA. 110 (2013) 16462–16467.

NIH-PA Author Manuscript

NIH-PA Author Manuscript

NIH-PA Author Manuscript

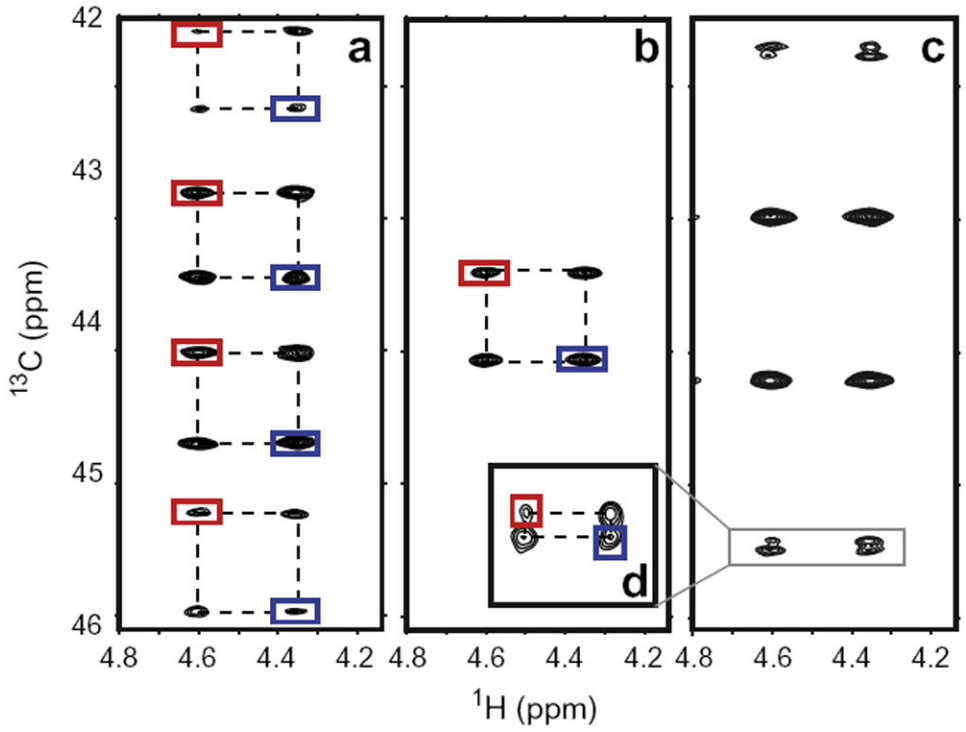

Fig. 3.

ZZ-exchange spectra for DMTCA aligned in poly-γ-benzyl-L-glutamate (PBLG) using a mixing time of 75 ms and T = 281.3 K. Auto-peaks are shown in red and blue boxes for the two methyl ^{13}C spins in DMTCA; cross peak patterns are indicated by dotted lines. (a) Coupled ZZ-exchange experiment in which cross peaks develop between individual multiplet component pairs reflecting both conformational differences in chemical shifts and RDCs. (b) Conventional ^{1}H decoupled ZZ-exchange experiment reflecting only differences in chemical shifts. (c) The case in which $\Delta\omega = 0$ is simulated by adding 180° ^{1}H and ^{13}C pulses in the midpoint of the t_1 frequency labeling delay. (d) Expansion of the boxed region in (c) shows that cross peaks are observed owing to difference in RDCs for the two exchanging methyl groups even in the absence of chemical shift differences.

NIH-PA Author Manuscript

NIH-PA Author Manuscript

NIH-PA Author Manuscript

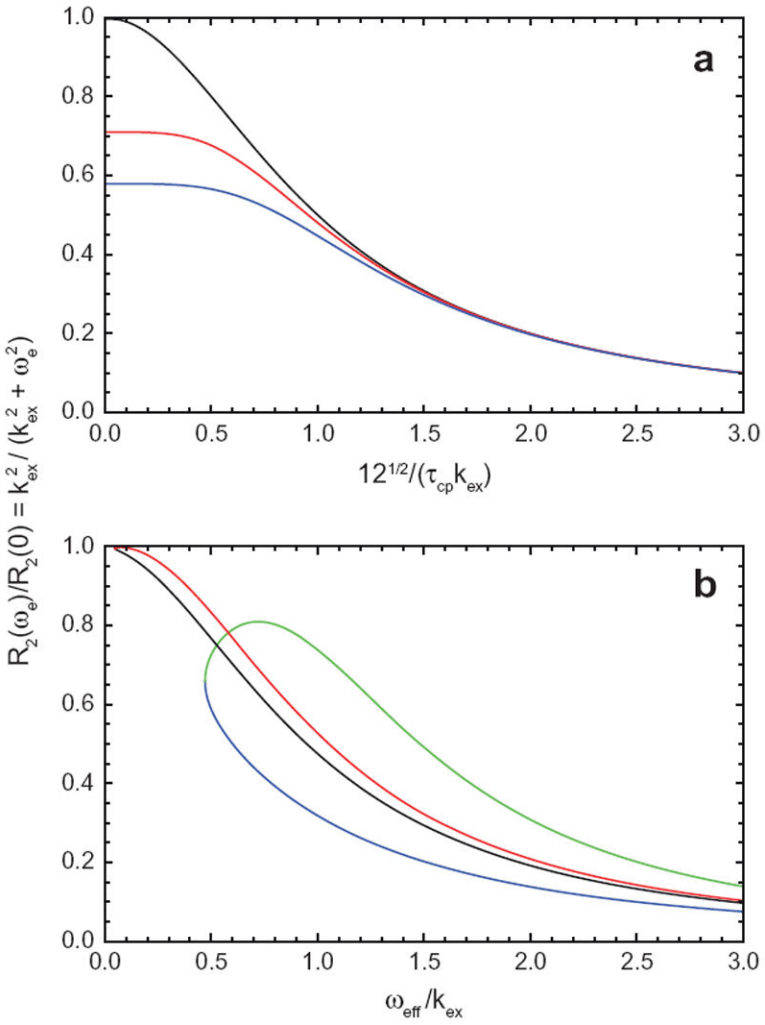

Fig. 4.

Normalized relaxation dispersion for (a) CPMG and (b) $R_{1\rho}$ experiments. Calculations were performed for a minor site population of $p_2 = 0.05$. In (a), the black curve shows the dispersion profile obtained in fast exchange ($\Delta\omega/k_{ex} = 0.28$) and is independent of scaling of $\Delta\omega$ for different static magnetic fields (and thus, as shown by Eq. (7), the full dispersion curve scales quadratically with the applied static magnetic field). The green and red curves show the profiles obtained for slow exchange; the static magnetic field for the green curve ($\Delta\omega/k_{ex} = 3.7$) is 1.33 times larger than for the red curve ($\Delta\omega/k_{ex} = 2.8$), as would be obtained using 600 and 800 MHz NMR spectrometers. The reduced dispersion amplitude for the green curve results, again using Eq. (7), with a full dispersion curve that scales less than quadratically with the applied static magnetic field. In (b), $\omega_1/2\pi = 150$ Hz, and $\Delta\omega = 3$ ppm, assuming a static magnetic field strength of 14.1 T (600 MHz). The green and blue curves show results for $k_{ex} = 2000\ s^{-1}$ in which the resonance offset from the population-averaged position is shifted (green) in the direction of the minor state resonance or (blue) away from the minor state resonance. The maximum in the green curve occurs when the spin-lock rf field is on-resonance with peak position in the minor chemical state. The red and black curves show that when $k_{ex} = 20{,}000\ s^{-1}$ is increased towards the fast-exchange limit, the

differences in (red, towards minor resonance) and (black, away from minor resonance) sweep directions is reduced.

NIH-PA Author Manuscript
NIH-PA Author Manuscript
NIH-PA Author Manuscript

NIH-PA Author Manuscript

NIH-PA Author Manuscript

NIH-PA Author Manuscript

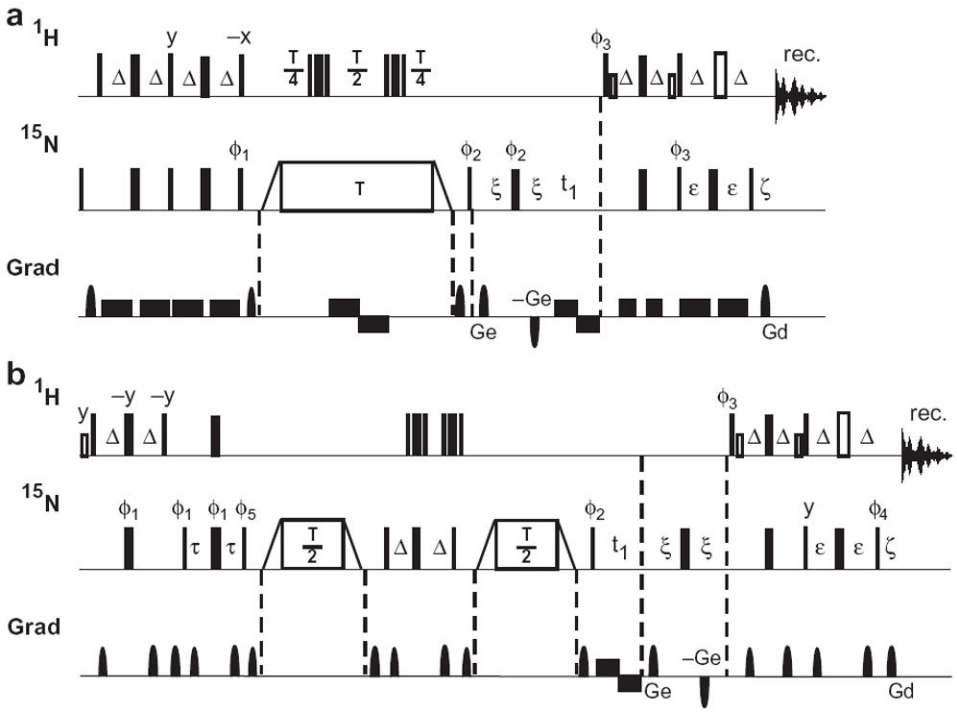

Fig. 5.

Pulse sequences for (a) TROSY-detected [82] and (b) TROSY-selected [83] $R_{1\rho}$ experiments. Narrow and wide bars depict 90° and 180° pulses, respectively; short narrow open bars represent water-selective 90° pulses; and wide open bars represent crafted 180° pulses that leave the water magnetization unperturbed [1]. Composite pulses are $90^\circ_x 210^\circ_y 90^\circ_x$, shown as three closely spaced bars. All pulses are *x*-phase unless otherwise indicated. The delays are $\Delta = 1/(4J_{NH})$, $\tau = 1/(8J_{NH})$, $\Xi >$ Ge, $\varepsilon = \Delta - \zeta/2$, $\zeta >$ Gd. The spin-lock fields are shown as open rectangles; the triangular segments are adiabatic pulse schemes to rotate the magnetization from (to) the *z*-axis to (from) the orientation of the effective field in the rotating frame [163]. Phase cycles are (a) $\varphi_1 = 4y, 4(-y)$; $\varphi_2 = y,x,-y,-x$; $\varphi_3 = y$; and receiver phase = $y,-x,-y,x,-y,x,y,-x$ and (b) $\varphi_1 = x,-x$; $\varphi_2 = x,x,-x,-x$; $\varphi_3 = y$; $\varphi_4 = x$; $\varphi_5 = 4(135°)\ 4(315°)$; and receiver = $(x,-x,-x,x,-x,x,x,-x)$. Gradients Ge and Gd are used for coherence selection; other gradients are for artifact suppression. Gradients are rectangular or shaped as indicated (for details see the original publications). Echo/antiecho quadrature detection [164] is achieved by (a) inverting φ_3, and the sign of gradient Ge and using $\varphi_2 = y,-x,-y,x$; and (b) inverting φ_3, φ_4, and the sign of gradient Ge. The φ_1 and receiver phases are inverted for each t_1 increment to shift axial peaks to the edge of the spectrum.

NIH-PA Author Manuscript

NIH-PA Author Manuscript

NIH-PA Author Manuscript

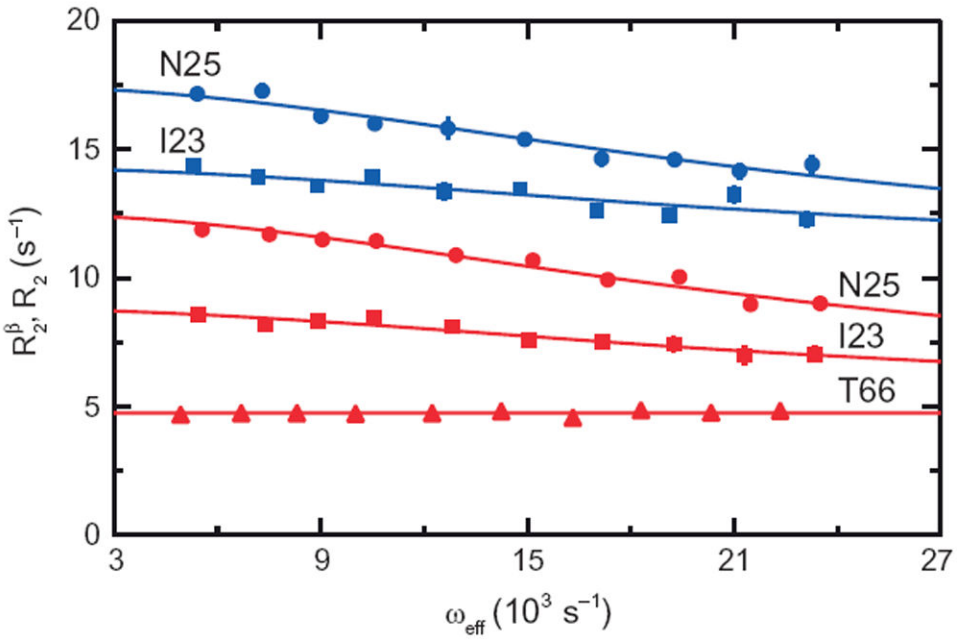

Fig. 6.

^{15}N $R_{1\rho}$ relaxation dispersion for ubiquitin. Relaxation dispersion curves for two exchange-broadened residues in ubiquitin, (circles) Asn 25 and (squares) Ile 23, collected using (blue) TROSY-detected or (red) TROSY-selected $R_{1\rho}$ experiments. Solid lines represent the fits to the experimental data obtained using the chemical exchange parameters of Massi et al. [86] and $R_2$0 or $R_2^{\beta,0}$ as an adjustable parameter. The $R_2^{\beta,0}$ values obtained in the TROSY-selected $R_{1\rho}$ experiment are 5.27 ± 0.05 s^{-1} and 5.62 ± 0.07 s^{-1} for Ile 23 and Asn 25, as compared to the R_2^0 values of 10.8 ± 0.1 s^{-1} and 10.6 ± 0.1 s^{-1} obtained in the TROSY-detected $R_{1\rho}$ experiment. Representative TROSY-selected $R_{1\rho}$ relaxation dispersion curve for one of the non-exchanging residues, Thr 66, is shown with triangles. Reprinted with permission from T.I. Igumenova, A.G. Palmer, Off-resonance TROSY-selected $R_{1\rho}$ experiment with improved sensitivity for medium- and high-molecular-weight proteins, J. Am. Chem. Soc. 128 (2006) 8110–8111. Copyright 2006 American Chemical Society.

NIH-PA Author Manuscript

NIH-PA Author Manuscript

NIH-PA Author Manuscript

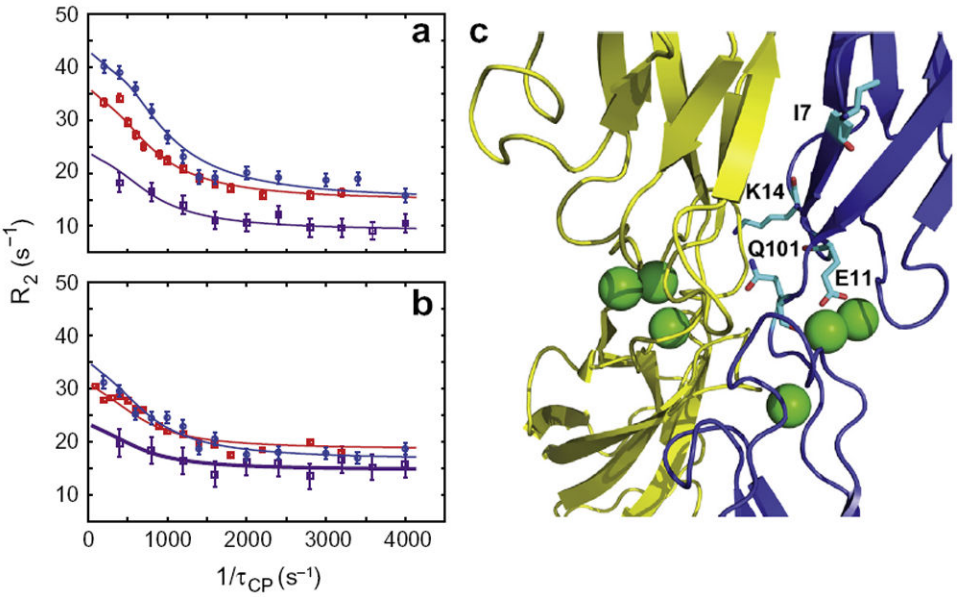

Fig. 7.

$^1H^N$ CPMG relaxation dispersion data for mouse E-cadherin extracellular domains 1 and 2. (a) Dispersion profiles for the monomer resonances of (a) Ile 7 and (b) Gln 101 for two different total monomer protein concentrations of (red, blue) 374 μM and (purple) 97 μM recorded at (red, purple) 600 and (blue) 800 MHz ^1H frequencies. The solid lines are fits to the data, yielding k_{ex} = 1890 ± 130 s^{-1} and p_2 = 0.025 ± 0.003 at the higher concentration at the lower concentration, p_2 = 0.017 ± 0.003. (c) X-dimer interface (drawn from the X-ray crystal structure of the E89A mutant, PDB ID code 3lni) with residues showing relaxation dispersion highlighted as stick representations. The green spheres represent bound calcium ions. Reprinted from Y. Li, N. Altorelli, F. Bahna, B. Honig, L. Shapiro, A.G. Palmer, Mechanism of E-cadherin dimerization probed by NMR relaxation dispersion, Proc. Natl. Acad. Sci. USA 110 (2013) 16462–16467.

NIH-PA Author Manuscript

NIH-PA Author Manuscript

NIH-PA Author Manuscript

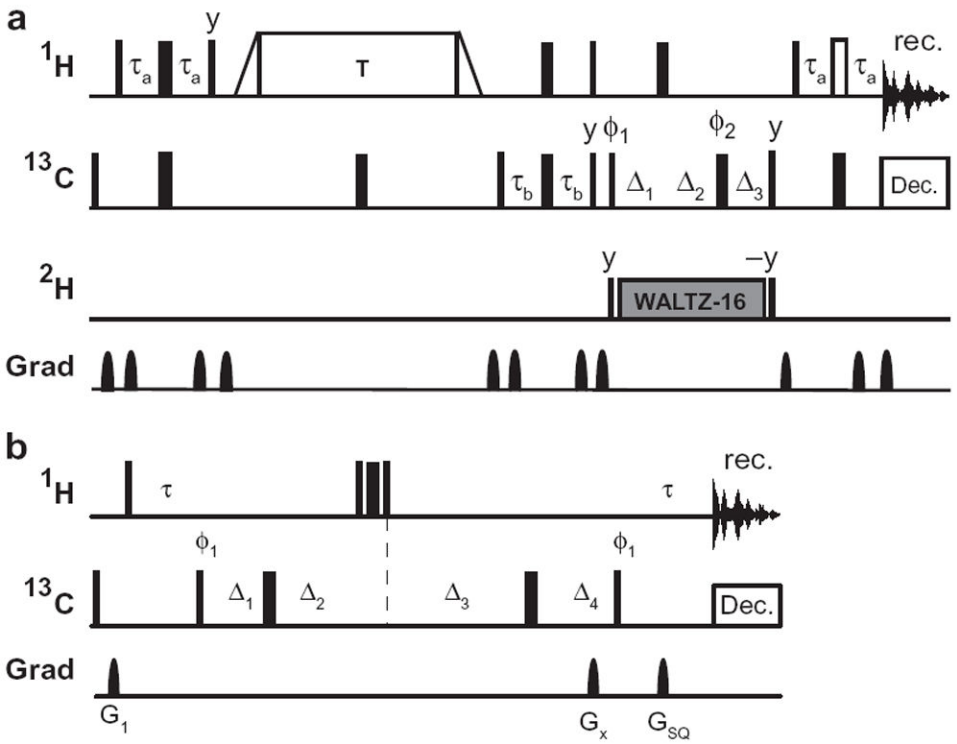

Fig. 8.

Relaxation measurements for methyl groups. (a) ^{1}H $R_{1\rho}$ pulse sequence for $^{13}CHD_2$ groups [17] and (b) ZQ-TROSY Hahn-echo pulse sequence for $^{13}CH_3$ groups [70]. Narrow and wide bars depict 90° and 180° pulses respectively; wide open bars represent crafted 180° pulses that leave the water magnetization unperturbed [1]. All pulses are *x*-phase unless otherwise indicated. Decoupling during acquisition uses WALTZ-16 [165]. (a) The delays are τ_a = 1.67 ms and τ_b = 2.0 ms. For constant time evolution, T_c = 14.3 ms, $\Delta_1 = \tau_b + t_1/2$, $\Delta_2 = T_c - \tau_b$, and $\Delta_3 = T_c - t_1/2$. For isolated $^{13}CHD_2$ methyl groups, non-constant time evolution uses $\Delta_1 = \tau_b + t_1/2$, $\Delta_2 = t_1/2$, and $\Delta_3 = \tau_b$. The spin-lock fields are shown as open rectangles; the triangular segments are adiabatic pulse schemes to rotate the magnetization from (to) the *z*-axis to (from) the orientation of the effective field in the rotating frame [163]. Phase cycles are $\varphi_1 = x,-x$; $\varphi_2 = x,x,y,y,-x,-x,-y,-y$; and receiver phase = $x,-x,-x,y,-y$. Gradients are for artifact suppression. Frequency discrimination is obtained by shifting the phase of the receiver and φ_1 according to the States-TPPI protocol [162]. (b) The delay $\tau = 1/(2J_{CH}) \approx 3.91$ ms. Phase cycles are $\varphi_1 = x,-x$; and receiver phase = $x,-x$. Gradients G_X and G_{SQ} are used for coherence selection; other gradients are for artifact suppression. For recording ZQ relaxation, $\varphi_1 = x$. Multiplet filtration is obtained by adding data sets recorded with (i) $\Delta_1 = 0$, $\Delta_2 = T/2 + \tau/4 + t_1$, $\Delta_3 = 0$ and $\Delta_4 = T/2 + \tau/4$ and (ii) $\Delta_1 = \tau/4$, $\Delta_2 = T/2 + t_1$, $\Delta_3 = \tau/4$ and $\Delta_4 = T/2$. The corresponding data sets for echo/antiecho quadrature detection use (iii) $\Delta_1 = 0$, $\Delta_2 = T/2 + \tau/4$, $\Delta_3 = 0$ and $\Delta_4 = T/2 + \tau/4 + t_1$ and (iv) $\Delta_1 = T/2$, $\Delta_2 = \tau/4$, $\Delta_3 = T/2 + t_1$ and $\Delta_4 = \tau/4$. Gradient $G_X = G_{ZQ}$ for data sets (i–iii) and G_{DQ} for data set (iv). The φ_1 and receiver phases are inverted for each t_1 increment to shift axial peaks to the edge of the spectrum. Corresponding values of parameters for measuring DQ relaxation rate constants are given in the original publication.

NIH-PA Author Manuscript

NIH-PA Author Manuscript

NIH-PA Author Manuscript

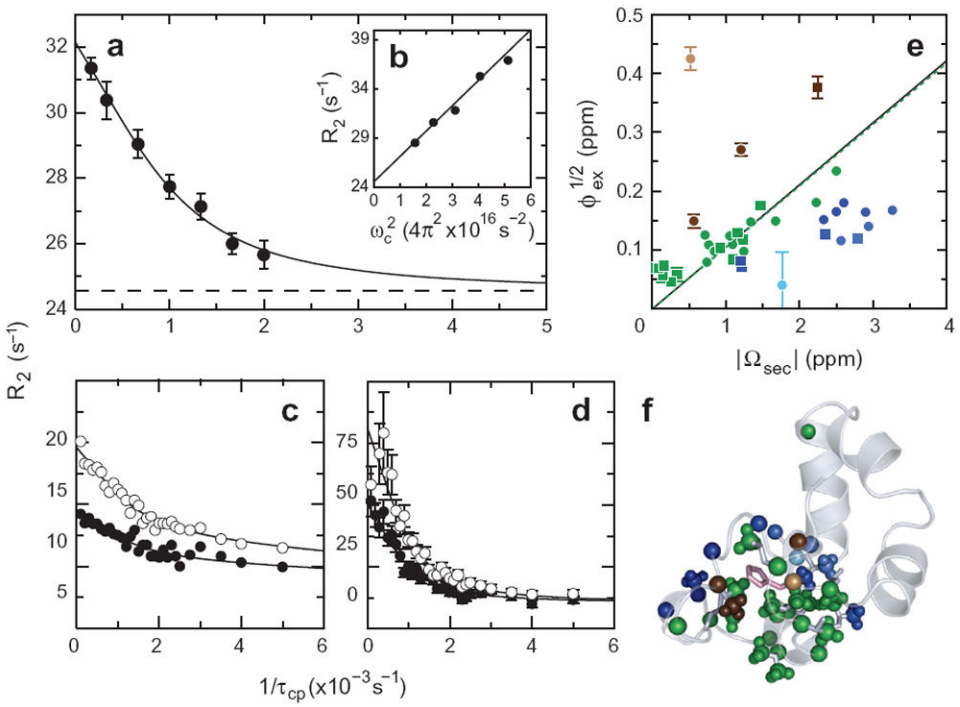

Fig. 9.

Relaxation dispersion characterization of a folding intermediate for the villin headpiece domain HP67. (a) Backbone $^{13}C^{\alpha}$ CPMG relaxation dispersion profiles for Arg 37 measured at a static magnetic field strength of 14.1 T. The solid lines are fits to the data. The dashed line corresponds to the value of R_2^0 used to constrain the data in the limit of infinitely fast pulsing. (b) The corresponding Hahn-echo R_2 dispersion data are plotted versus ω_c^2 in the inset; the solid line is a linear fit to the data; the *y*-intercept determines R_2^0. Methyl ^{13}C CPMG relaxation dispersion profiles measured at static magnetic field strengths of (○) 14.1 T and (●) 18.8 T for (c) Val20 $C^{\gamma 2}$ and (d) Val33 $C^{\gamma 2}$. The solid lines are fits to the data. (e) Analysis of $\varphi_{ex} = p1p2\Delta\omega 2$ for $^{13}C^{\alpha}$ and methyl ^{13}C spins in HP67. Values determined from individual fits of R_{ex} and the global value of k_{ex} = 3190 ± 180 s^{-1} are plotted versus $|\Omega_{sec}|$ for (a) $^{13}C^{\alpha}$ (●,○) and (b) methyl ^{13}C (■,□) spins. Green symbols represent data for residues that are assumed to be fully unfolded in the intermediate ensemble; the dashed green line yields a slope of 0.104 ± 0.005, corresponding to a population of (1.09 ± 0.11)% for the intermediate state. The solid line has a slope of 0.0105, corresponding to p_2 = (1.11 ± 0.09)% observed previously for ^{15}N spin relaxation dispersion [101]. Data points that were excluded from the fit are grouped into two categories: (i) those that lie above and to the left of the fitted line adopt non-native conformations in the intermediate and (ii) those that lie below and to the right of the fitted line maintain residual native-like interactions in the intermediate. Residues in (i) and (ii) are colored with brown and blue gradients, respectively, with the color of the data points becoming lighter as the ratio $|\Delta\delta/\Omega_{sec}|$ deviates from unity, in which $|\Delta\delta|$ was obtained from φ_{ex} assuming p_2 = (1.11 ± 0.09)%. (f) Exchange broadened $^{13}C^{\alpha}$ and ^{13}C methyl groups are mapped onto the structure of HP67. Atoms are colored to correlate with the classifications depicted in (e). Two regions of residual interactions are maintained the intermediate: (i) at the interface of the N- and C-terminal

subdomains and (ii) in the vicinity of His41. Reprinted from N.E. O'Connell, M.J. Grey, Y. Tang, P. Kosuri, V.Z. Miloushev, D.P. Raleigh, A.G. Palmer, Partially folded equilibrium intermediate of the villin headpiece HP67 defined by ^{13}C relaxation dispersion, J. Biomol. NMR 45 (2009) 85–98, with permission from Springer.

NIH-PA Author Manuscript
NIH-PA Author Manuscript
NIH-PA Author Manuscript

NIH-PA Author Manuscript

NIH-PA Author Manuscript

NIH-PA Author Manuscript

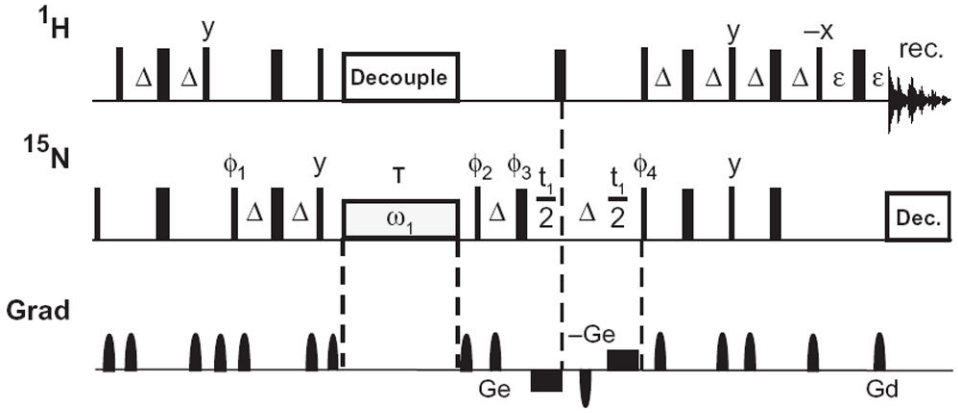

Fig. 10.

^{15}N CEST/DEST pulse sequence [103]. Narrow and wide bars depict 90° and 180° pulses, respectively. All pulses are *x*-phase unless otherwise indicated. The ^{1}H transmitter is positioned on the water resonance throughout the sequence except during the relaxation period *T*, when it is moved to the center of the amide region (8.4 ppm). The ^{15}N transmitter is placed at 119 ppm except during *T*, when it is relocated to the desired offset. A coherent decoupling train consisting of $90_x240_y90_x$ pulses is used for ^{1}H decoupling during *T* for CEST experiments; decoupling can be obtained with two composite 180° pulses as in Fig. 5 for DEST experiments. In the CEST experiment, temperature compensation is obtained by applying the ^{1}H decoupling scheme for a time $T_{max} - T$ immediately after the completion of acquisition, in which T_{max} is the maximum exchange time used in the experiment (typically $T = T_{max}$ or 0). ^{15}N decoupling during acquisition is achieved with WALTZ-16 [165]. Delays are $\Delta = 1/(4J_{NH})$, and $\varepsilon >$ Gd. The phase cycle is $\varphi_1 = \{x, -x\}$, $\varphi_2 = \{y\}$, $\varphi_3 = \{2x,2y, 2(-x), 2(-y)\}$, $\varphi_4 = \{x\}$, receiver = $\{x, -x, -x,x\}$. Weak bipolar gradients, depicted as solid black bars, are applied during the t_1 period. Unlabeled gradients are used to suppress unwanted coherences and artifacts, whereas Ge and Gd are encoding and decoding gradients, respectively, for echo/antiecho coherence selection, obtained by inverting the signs of φ_4 and Ge [164]. Values of φ_2 and the receiver phase are inverted between t_1 points to shift axial peaks to the edge of the spectrum. A conventional HSQC-detected $R_{1\rho}$ pulse sequence is obtained by replacing the ^{1}H decoupling and ^{15}N spin-lock during *T* with the scheme (including the adiabatic sweeps) shown in Fig. 5a.

NIH-PA Author Manuscript

NIH-PA Author Manuscript

NIH-PA Author Manuscript

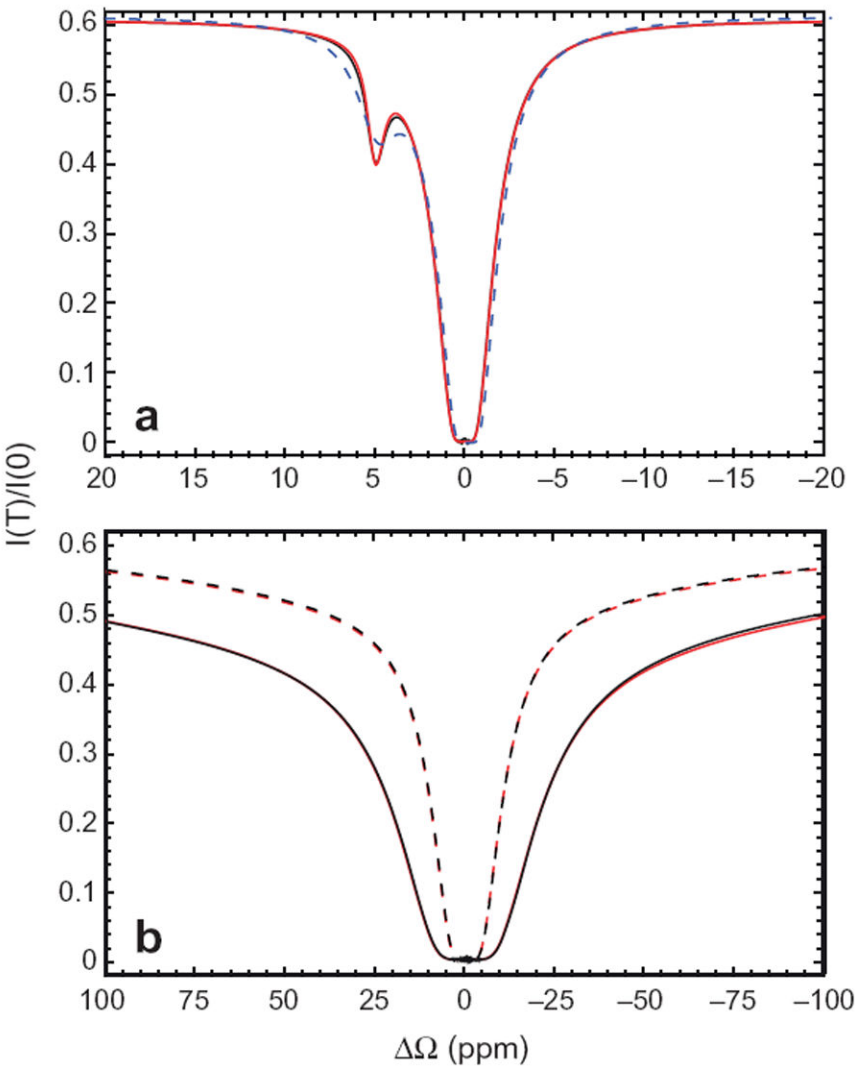

Fig. 11.

Theoretical (a) CEST and (b) DEST profiles. Calculations assumed k_{ex} = 50 s^{-1}, p_2 = 0.015, Ω_1 = −0.076 ppm, Ω_2 = 5 ppm, and T = 0.48 s. $\Delta\Omega$ is measured relative to the population-averaged resonance position. In (a) $R_{11} = R_{12}$ = 1 s^{-1}, $R_{21} = R_{22}$ = 20 s^{-1}, $\omega_1/2\pi$ = 25 Hz. In (b) R_{22} = 20,000 s^{-1} and (dashed) $\omega_1/2\pi$ = 150 Hz and (solid) $\omega_1/2\pi$ = 300 Hz. Black lines give the numerical solutions of the Bloch–McConnell equations (Eqs. (2)-(4) and (10)) and red lines give the $R_{1\rho}$ approximations using (a) Eqs. (7)-(9) and (12) or (b) Eqs. (7)-(9), (11) and (12). The blue dashed line in (a) shows the result of increasing R_{22} = 200 s^{-1} in the CEST experiment, calculated using Eqs. (7)-(9), (11), and (12) as for the DEST experiment.